Fuel 334 (2023) 126789

Contents lists available at ScienceDirect

Fuel

journal homepage: www.elsevier.com/locate/fuel

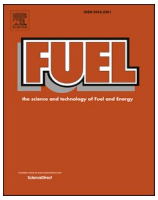

Full Length Article

Analysis by temperature-programmed reduction of the catalytic system Ni-Mo-Pd/Al_2O_3

Ivan Pedroarena, Lucía Grande, Jonathan J. Torrez-Herera, Sophia A. Korili, Antonio Gil *

INAMAT˜2, Departamento de Ciencias, Universidad Pública de Navarra, Campus de Arrosadía, 31006-Pamplona, Spain

ARTICLE INFO

Keywords:
Temperatura-programmed reduction
Promoted alumina catalyst
Nickel molybdenum catalyst
Nickel palladium catalyst

ABSTRACT

Alumina-supported nickel catalysts are used to facilitate many reactions at various scales. However, the deactivation of these catalysts is an important problem that has prompted the search for solutions such as the addition of other metals that act as promoters. In this research, the interactions that form between the support and the metals have been studied, a fundamental property that directly affects the performance of the catalyst. With this idea, several Ni-Pd and Ni-Mo bimetallic and various Ni-Mo-Pd trimetallic samples have been prepared, and the reduction capacity of the oxide phases by temperatura-programmed reduction has been analyzed and studied. It has been found that in bimetallic catalysts, Pd favors the appearance of NiO species that are more easily reducible than Mo. In the same way, the data obtained from the trimetallic simples suggest that the impregnation order of Mo and Pd is not a determining factor in these catalysts. In addition, it has been found that the co-impregnation of Ni with Pd gives better results than the sequential impregnation of these metals. The results obtained have also shown that the order of nickel impregnation is decisive. In the case of Ni-Mo catalysts, by impregnating the molybdenum first, catalysts with better reducing properties can be obtained.

1. Introduction

Transition metals have been widely studied due to their numerous applications, such as catalysts in a wide variety of industrial processes involving reduction atmosphere and the activation or conversion of hydrocarbons [1–3]. The catalytic performance is determined by the chemical structure of the catalyst and its properties [4]. The success or not of the preparation or modification of the catalysts depends on the availability of adequate characterization technology, that is, on the techniques to determine the condition of the catalyst. One of the most important challenges in the field of metal catalysis is the synthesis of metal particles with narrow size distributions and homogeneous physicochemical properties that allow clear relationships to be established between reactivity and structure [5].

Supported nickel catalysts have been widely used in industry as they can catalyze many useful reactions such as methanation, hydrogenation, hydrocracking and dry/steam reforming [5,6]. Various authors have shown that the performance and specificity of these catalysts depend on the interaction between the metal and the support [7–13]. Han *et al.* [8] studied the effect of Ni particle size and the nature of the support using various supports as SiO_2, Al_2O_3, MgO, ZrO_2 and TiO_2. The catalytic behaviour evolved in the dry reforming of methane as follows: NiO/Al_2O_3 ≥ Ni/MgO > Ni/SiO_2 > Ni/ZrO_2 > Ni/TiO_2. This evolution was attributed to the effect of the supports on the reaction. Zhang *et al.* [9] also observed the following evolution in the catalytic behavior: Al_2O_3 modified with NiO/MgO > Ni/MgO > Ni/SiO_2 > Ni/Al_2O_3 > Ni/ZrO_2 > Ni/TiO_2. The higher catalytic performance of Al_2O_3 modified with NiO/MgO was related to the strong metal-support interaction (SMSI) effect and the size of the well-dispersed Ni particles. The techniques that make it possible to demonstrate the interaction between the metal and the support are, for example, XRD, XPS, ISS and TPR [6]. Generally, alumina is used as a support in these catalysts due to its thermal stability under the reaction conditions. However, catalysts can undergo deactivation processes due to carbon formation reactions, which dirty the catalyst surface and affect catalytic behavior [14,15]. For these reasons, much effort has been devoted to improve the performance of Ni-based catalysts by incorporating various promoters. Among them, noble metals such as Pt, Pd or Rh and other transition metals such as Mo, Co, La or Mn can be highlighted [16].

Nickel molybdate is a promising catalyst for many reactions such as hydrotreating processes, oxidative dehydrogenation (ODH), and selective oxidation of light alkanes [17–19]. Especially, these catalysts are

* Corresponding author.
E-mail address: andoni@unavarra.es (A. Gil).

https://doi.org/10.1016/j.fuel.2022.126789
Received 20 June 2022; Received in revised form 21 August 2022; Accepted 13 November 2022
Available online 19 November 2022

among the most used in hydrodenitrogenation or hydrodesulfurization processes, one of the most important processes in oil refinin [18,20–24] as well as hydrodeoxygenation, a promising technique to reduce oxygenated compounds present in the biocrude obtained from waste [22,23,25,26]. Supported nickel molybdenum catalysts are generally prepared by depositing molybdenum and nickel oxides on the surface of supports such as alumina (Al_2O_3) and silica-alumina (SiO_2-Al_2O_3) [20,27–29]. Many studies have focused on the nature and structure of Mo species, and the results of studies employing various characterization techniques indicate that the presence of promoters does not greatly affect the state of Mo species on the Al_2O_3 surface [20,27]. According to the literature, these bimetallic catalysts are active, both reduced and sulfided [25,30,31], with nickel-molybdenum contents generally of 3–12 wt% Ni and 5–20 wt% Mo [20,28–30,32–34].

Although the trend in recent years is to use catalysts made of non-noble metals, which are stable thermically and cheap, catalysts based on noble metals such as Pt, Pd or Ru are still used in many reactions, such as hydrogenation, hydrodeoxygenation, hydrodechlorination or reforming of methane [35–41]. The reasons why these catalysts remain interesting despite being expensive are that they generally have better performance and are less sensitive to deactivation by coke formation [25,40,42]. Among the most used supports, alumina (Al_2O_3), silica (SiO_2) or activated carbon can be highlighted [37,38,40,41,43–46]. Mixing Pd with a second metal component to form bimetallic catalysts can improve catalytic performance (activity, durability, and selectivity) while reducing catalyst cost [47,48]. The oxidation state of the catalyst metals and the distribution of the nanoparticles are two of the most important factors affecting the catalytic performance [49]. Among Pd-based bimetallic systems, palladium-nickel (Pd-Ni) is one of the most investigated due to its excellent performance compared to monometallic Pd or Ni catalysts [41]. The high performance of these catalysts is largely due to the ability of Pd to absorb large amounts of molecular hydrogen at room temperature [50]. Nickel-palladium catalysts generally contain about 10 wt% Ni and about 0.5 wt% Pd [36,37,40].

Metal oxides supported on inert materials such as SiO_2 or Al_2O_3 might exhibit different reduction behaviors compared with unsupported oxides. The reduction can be enhanced or limited depending on the characteristics of the interaction between the metal and the support [51]. For example, as a result of this interaction related to the thermal treatment and the solid state reaction, metal aluminates can be formed which are hardly reducible [52]. In other cases, a decrease in the metal oxide reduction temperature has been described thanks to this interaction with the support. This phenomenon is due to the ability of the support to act as a dispersing agent for the oxide particles. That is, if the metal oxides are homogeneously distributed along the surface of the support, their reduction is easier than if they are forming large agglomerates. Another factor that notably affects the reduction of metal oxides is the presence of foreign metal species [51].

The reduction capacity of the oxide phases of the metals present in the catalysts is a fundamental property, since the performance of the catalyst generally depends on it [53–55]. Therefore, this work has focused on studying the effect that variations in the production process and changes in loading ratios can have on the species of various catalysts, as well as on their reduction capacity. For this, bimetallic Ni-Pd and Ni-Mo catalysts supported on Al_2O_3 have been prepared using wet impregantion and two methodologies, sequential impregnation and co-impregnation of the metals from aqueous solutions. Furthermore, in order to study the effect of adding a third metal, trimetallic catalysts have been generated by adding the remaining metal (Mo or Pd). Temperature-programmed reduction (TPR) has been shown to be a sensitive technique to study reducibility and it has been applied successfully for characterization of NiO/Al_2O_3, MoO_3/Al_2O_3 and PdO/Al_2O_3 catalyst [20,32,35–37,53,56–60]. In addition, it is a technique that does not depend on any specific property of the catalyst other than that the species under study be in a reducible condition [51]. The use of TPR profiles provide fingerprints of the chemical nature and environment of the catalytic component [61]. Therefore, TPR was used to elucidate the phases of Ni, Mo and Pd species in the catalysts.

2. Experimental section

2.1. Materials and catalyst preparation

The materials used for the synthesis of the catalysts included γ-Al_2O_3 (Rhône-Poulenc), nickel nitrate hexahydrate (≥97 %, Merck), ammonium molybdate tetrahydrate, (99.98 %, Sigma-Aldrich) and a solution of palladium(II) nitrate in nitric acid (Merck).

The synthesis of the catalysts was performed using the conventional wet impregnation method. However, the impregnation was carried out considering two ways in order to study the effect that variations in the preparation method may have on the reducibility of the catalyst. Firstly, the catalysts were prepared by successive individual impregnations. First of all, nickel nitrate hexahydrate salt was dissolved in distilled water. This solution was then added dropwise to the measured quantity of γ-Al_2O_3 with constant stirring for about 1 h. The wet catalyst was then dried 1 h at room temperature and 16 h at 90 °C. The dry catalyst was finally calcined for 4 h at 550 °C (Ni(10 %)/Al_2O_3). Next, successive impregnations were carried out following these same steps but using a solution of distilled water and ammonium molybdate tetrahydrate until the desired percentage of molybdenum was obtained (Ni(10 %)-Mo(X %)/Al_2O_3). In the case of Ni-Pd catalysts, instead of dissolving a salt in water, a solution of Pd(II) in nitric acid was added to the Ni/Al_2O_3 sample (Ni(10 %)-Pd(Y%)/Al_2O_3). Therefore, Ni-Mo/Al_2O_3 catalysts were prepared whose molybdenum content ranges (X%) from 3.5 to 16 wt%, while the percentage of Pd in Ni-Pd/Al_2O_3 catalysts ranges (Y%) from 0.07 to 0.46 wt%. All catalysts have the same amount of nickel, 10 wt%. Finally, two bimetallic catalysts were chosen and a third impregnation was carried out with the remaining metal, giving rise to the following catalysts: Ni(10 %)-Pd(0.13 %)-Mo(8.6 %)/Al_2O_3 and Ni(10 %)-Mo(8.6 %)-Pd(0.13 %)/Al_2O_3. The two bimetallic catalysts on which the third metal was incorporated were selected because they had intermediate amounts of the promoter metal that are clearly seen in the characterizations carried out.

Ni-Pd and Ni-Mo bimetallic catalysts were also prepared by co-impregnation. In this case, both the nickel nitrate hexahydrate and the other precursor (ammonium molybdate tetrahydrate or palladium(II) nitrate) were dissolved in the same aqueous solution. That is, both metals were impregnated on the support at the same time. To achieve the trimetallic catalysts, a second impregnation was performed on the co-impregnated samples. The catalysts generated by co-impregnation contain 10 Ni, 0.13 Pd and 8.6 wt% Mo and they are denoted as [Ni(10 %)-Pd(0.13 %)]/Al_2O_3, [Ni(10 %)-Mo(8.6 %)]/Al_2O_3, [Ni(10 %)-Pd(0.13 %)]-Mo(8.6 %)/Al_2O_3 and [Ni(10 %)-Mo(8.6 %)]-Pd(0.13 %)/Al_2O_3. The impregnation processes are schematically represented in Fig. 1.

In order to evaluate the effect of nickel content, a catalyst with 20 wt % nickel supported on alumina has also been prepared (Ni(20 %)/Al_2O_3). Subsequently, successive individual impregnations of Mo or Pd have been carried out on this catalyst, until the desired percentages have been achieved (Ni(20 %)-Mo(8.6 %)/Al_2O_3 and Ni(20 %)-Pd(0.13 %)/Al_2O_3). Finally, to study the effect of the order of impregnation of the metals, two bimetallic catalysts were prepared impregnating molybdenum and palladium first (Mo(8.6 %)-Ni(10 %)/Al_2O_3 and Pd(0.13 %)-Ni(10 %)/Al_2O_3).

2.2. Temperature-programmed reduction

Temperature-programmed reduction studies were performed using a Micromeritics TPR/TPD 2900 equipment instrument. TPR tests were carried out from room temperature to 1000 °C at a heating rate of 10 °C/min, under a total flow of 30 cm^3/min (5 % H_2 in Ar, Praxair). Previously, the fresh catalysts were pretreated at 200 °C for 2 h under a flow

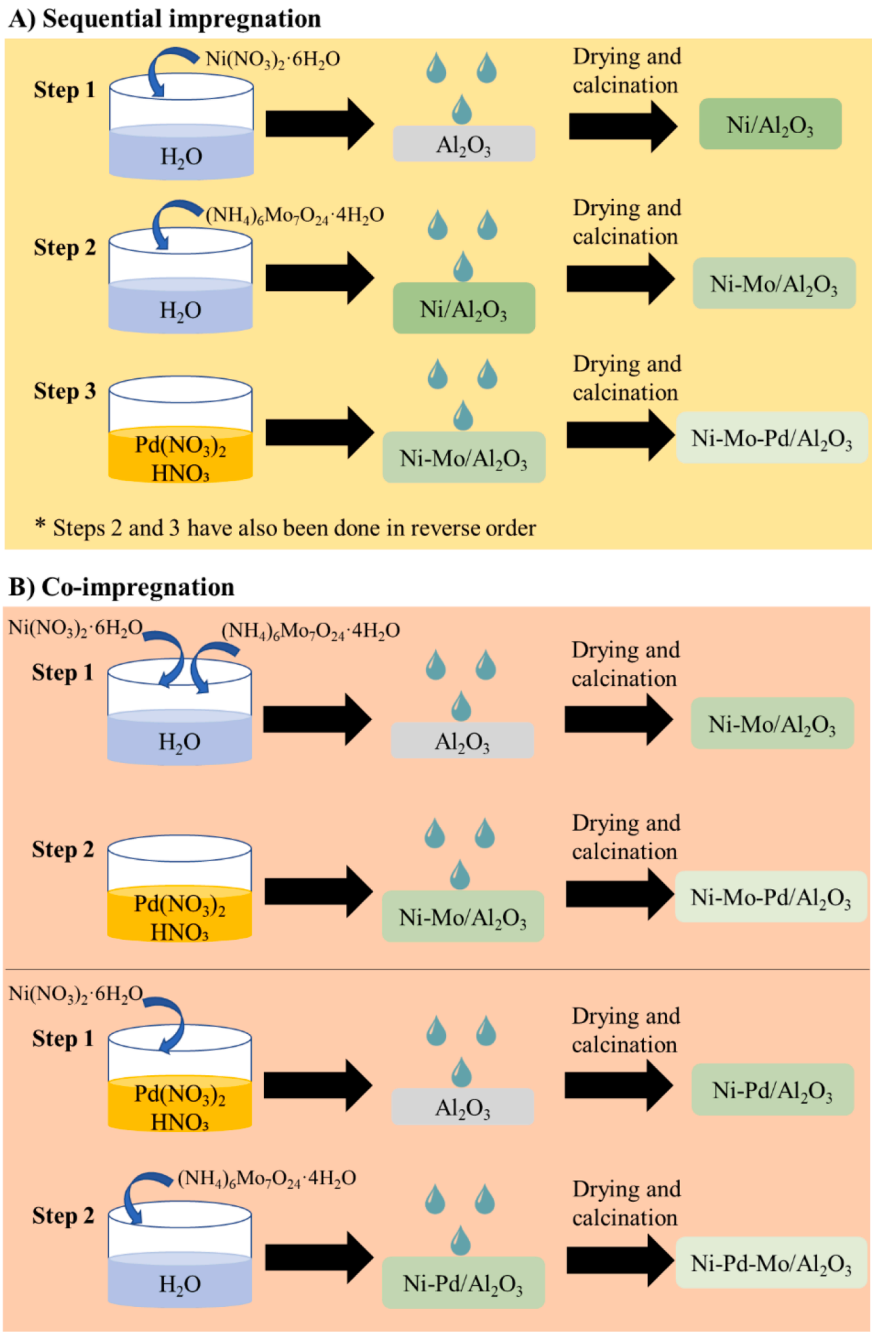

Fig. 1. Schematic diagram of preparation processes of A) seq-impregnated and B) co-impregnated catalysts.

of He (Nippon Gases) to remove water and other contaminants. All TPR profiles were normalized for the same catalyst mass (25 mg).

2.3. Powder X-ray diffraction (XRD)

The structural phases were analyzed using an X-ray diffractometer (model Siemens D5000) equipped with an Ni-filtered CuKα radiation source ($\lambda = 0.1548$ nm) at a scanning speed of 1°/min over the 2θ range of 10-80°. The phase identification was made by comparison to the International Centre for Diffraction Data (ICDD).

3. Results and discussion

3.1. Temperature-Programmed reduction analysis of samples generated by sequential individual impregnations

From the maximum reduction peak, the NiO species are classified into four types: α, β_1, β_2 and γ [60,62]. In the α group are the NiO species that have a weak interaction with the support and have reduction temperatures of between 300 and 500 °C (NiO-free species). The β_1-type is assigned to nickel oxide species (NiO plus Ni in a mixed oxide phase) that interact weakly or slightly with the support and are reduced between 500 and 600 °C [63]. β_2-type is less reducible NiO in Al-rich stable phase with the reduction temperature between 600 and 750 °C. Finally, a much less reducible NiO species belongs to the γ type (750–850 °C) [55,58]. From the results included in Figs. 2 and 3, the Ni(10 %)/Al_2O_3

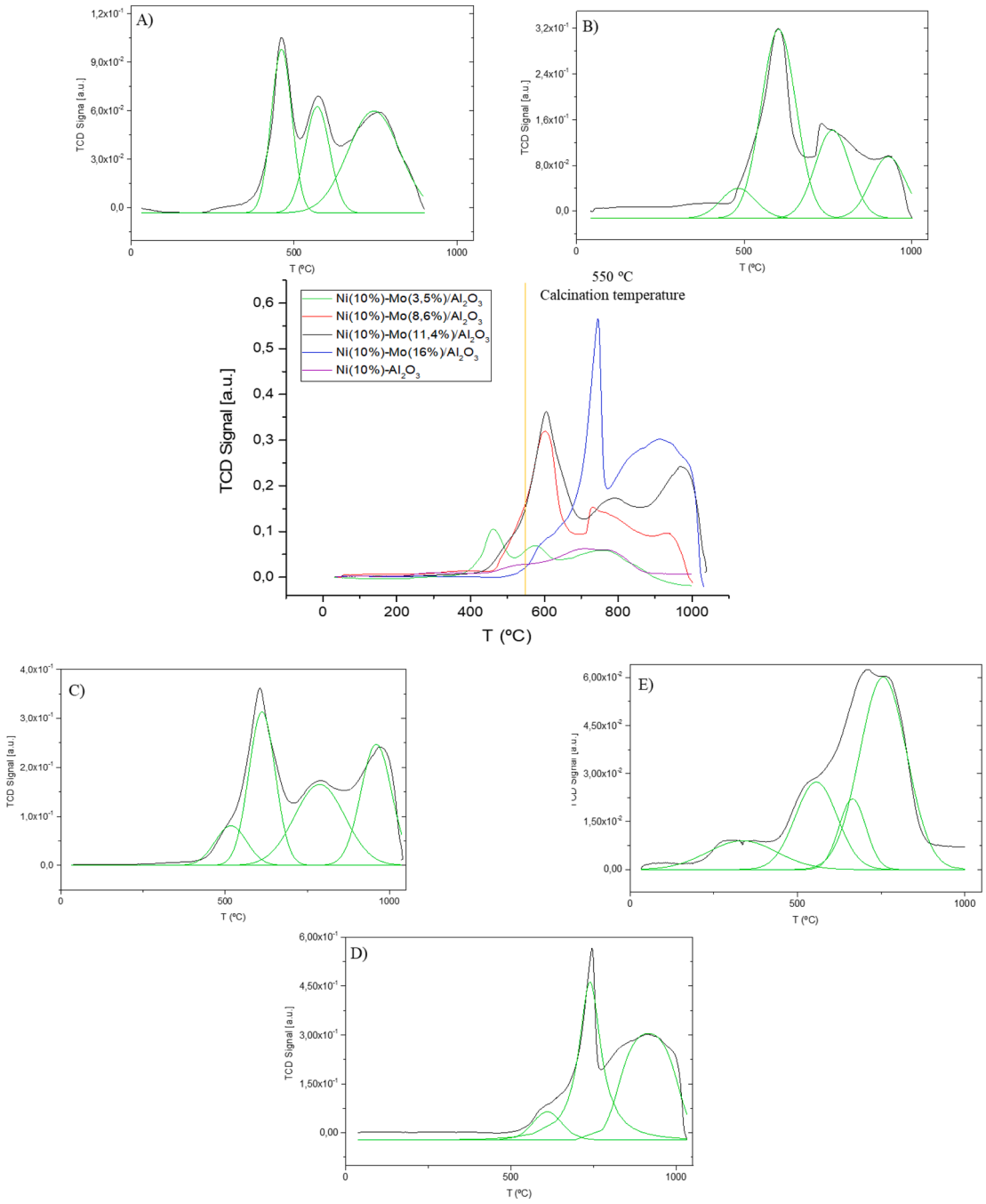

Fig. 2. TPR patterns of Ni/Al_2O_3 and four $Ni\text{-}Mo/Al_2O_3$ samples. All catalysts were previously calcined at 550 °C. Peak deconvolution of: A) Ni(10 %)-Mo(3.5 %)/Al_2O_3; B) Ni(10 %)-Mo(8.6 %)/Al_2O_3; C) Ni(10 %)-Mo(11.4 %)/Al_2O_3; D) Ni(10 %)-Mo(16 %)/Al_2O_3; E) Ni(10 %)-Al_2O_3. The TPR patterns comparison is included in the central Figure.

catalyst synthesis in this work exhibited three characteristic reduction peaks at T_{max} of 335, 556 and 756 °C. The first peak at 335 °C is characteristics of the reduction of NiO with a weak interaction with support. The second reduction peak at 556 °C is due to the reduction of dispersed β_1-type NiO with a stronger interaction with the support. The third reduction peak at 756 °C is attributed to the reduction of $NiAl_2O_4$. In addition, a small peak is observed at a temperature of 664 °C, which probably corresponds to β_2-type NiO species. These data accord to previous characterizations results of catalysts of this type reported by several authors [16,26,64,65]. The maxima temperature and the areas of the peaks obtained after the deconvolution of the TPR curves of Ni(10 %)/Al_2O_3 and Ni(10 %)-Mo(X%)/Al_2O_3 catalysts are included in Table 1. It must be taken into account that the peaks that occur from the calcination temperature of the catalysts (550 °C) are affected by the changes of phase and structure that the support undergoes, since at those temperatures the support and metals form new compounds.

The TPR profile of the four calcined $Ni\text{-}Mo/Al_2O_3$ catalysts with various percentage of molybdenum can be observed in Fig. 2. The deconvolution of the overlapping peaks (using a Gaussian fit) present in the TPR patterns of the four catalysts can be seen in Fig. 2A, 2B, 2C and 2D. The results show how the interaction with the support increases in catalysts with a higher percentage of molybdenum, causing the reduction temperatures to be higher (see T_{max} included in Table 1). From the results obtained for other authors [16,17,26,32,33,66], it can affirm that the first reduction peaks that appear between 462 and 507 °C in the samples is related to the reduction of α-type NiO. The peaks that appear

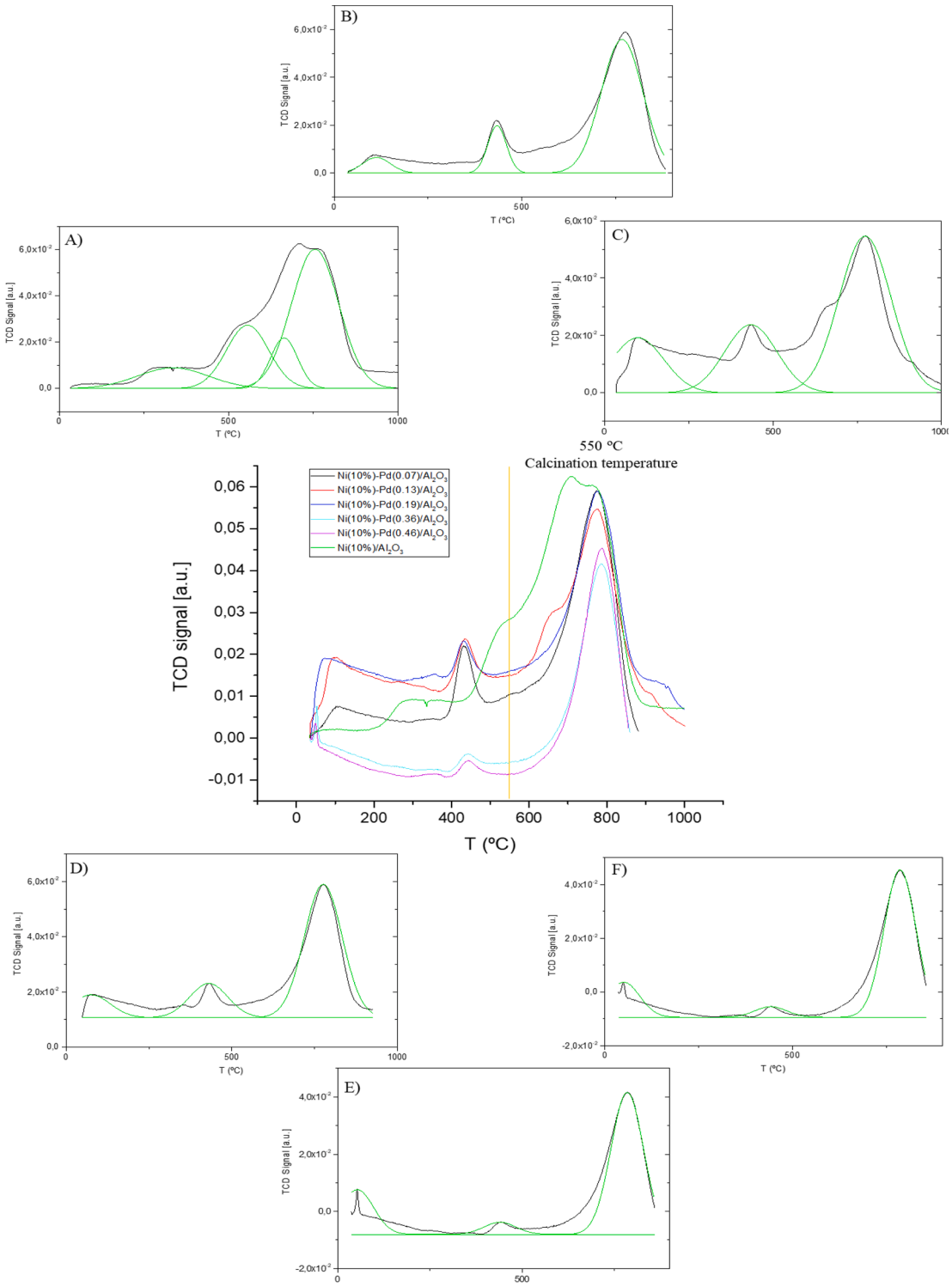

Fig. 3. TPR patterns of Ni/Al_2O_3 and $Ni\text{-}Pd/Al_2O_3$ samples. All catalysts were previously calcined at 550 °C. Peak deconvolution of: A) Ni(10 %)/Al_2O_3; B) Ni(10 %)-Pd(0.07 %)/Al_2O_3; C) Ni(10 %)-Pd(0.13 %)/Al_2O_3; D) Ni(10 %)-Pd(0.19 %)/Al_2O_3; E) Ni(10 %)-Pd(0.36 %)-Al_2O_3; F) Ni(10 %)-Pd(0.46 %)-Al_2O_3. The TPR patterns comparison is included in the central Figure.

between 571 and 610 °C, correspond to the reduction of β_1-type NiO, MoO_3 and $NiMoO_4$ species. In the catalysts that present 3.5, 8.6 and 11.4 wt% of Mo, these first peaks can be seen intensely, while in the sample with the highest percentage of molybdenum, these peaks are hardly seen as the MoO_2 reduction peak increases significantly (reduction temperatures between 744 and 787 °C, see Table 1). The peak corresponding to the reduction of the α-type NiO species presents a similar area and intensity in the catalysts with 3.5, 8.6 and 11.4 wt% of molybdenum (see Table 1 and Fig. 2**A, 2B and 2C**). As the amount of molybdenum increases, the peak generated by the reduction of the MoO_3 and $NiMoO_4$ species increases. The reduction of the intensity of the NiO peaks as the intensity of the $NiMoO_4$ peaks increases has also been previously described by other authors [16,26]. In a study by Fan *et al.* [67] obtained similar results and confirmed that increasing the

Table 1
Maximum temperature and the areas of the peaks obtained after the deconvolution of the TPR curves of Ni(10%)/Al_2O_3 and Ni(10%)-Mo(X%)/Al_2O_3 catalysts.

Catalyst	α-NiO		β_1-NiO/MoO_3/$NiMoO_4$		MoO_2/$NiAl_2O_4$		$Al_2(MoO_4)_3$	
	T max (°C)	Peak area [a.u.]	T max (°C)	Peak area [a.u.]	T max (°C)	Peak area [a.u.]	T max (°C)	Peak area [a.u.]
Ni(10 %)/Al_2O_3	335	0.8	556	2.9	756	14.2	–	–
Ni(10 %)-Mo(3.5 %)/Al_2O_3	462	11.8	571	5.6	744	18.5	–	–
Ni(10 %)-Mo(8.6 %)/Al_2O_3	482	6.6	603	42.9	764	20	931	14.1
Ni(10 %)-Mo(11.4 %)/Al_2O_3	507	7.3	605	44.6	787	21.2	971	29.8
Ni(10 %)-Mo(16 %)/Al_2O_3	–	–	610	13.6	738	74.2	915	40.9

amount of Mo in Ni-Mo catalysts increases the NiO reduction temperature, due to the strong interaction of Ni and Mo.

The peak that is located between 744 and 787 °C in the four Ni-Mo/Al_2O_3 catalysts, correspond to the reduction of $NiAl_2O_4$ and MoO_2 to Mo and increases in intensity as the percentage of molybdenum is higher. That is, in this temperature range, both the reduction of MoO_2 to MoO and the reduction of MoO to metallic Mo have been described [26,33,68]. It is reported that $NiAl_2O_4$ species begin to form at calcination temperatures above 500 °C. The interaction between Al_2O_3 and NiO is caused by the dissolution and incorporation of Al^{3+} ions in NiO crystallites which makes it difficult to break the Ni-O bond [69]. The last reduction peak that appears between 730 and 970 °C is caused by the reduction of $Al_2(MoO_4)_3$ [20,26]. In the same way as with the previous peak, the intensity and the area corresponding to this peak increase as the amount of molybdenum in the samples increases, whereas in the TPR curve of the catalyst with 3.5 wt% of this metal, no peak is found at that temperature.

The data included in Table 1 show how the addition of small amounts of Mo favors the reduction of nickel. By adding this promoter metal, NiO peak areas increase significantly. However, in catalysts with a high wt.% Mo, this effect is lost and the area of the more difficultly reducible NiO species increases. These data seem to indicate that by adding large amounts of molybdenum, the interaction between the metal oxides and the support increases, losing the promoting effect.

The TPR profiles of calcined Ni-Pd/Al_2O_3 samples, in which three well defined peaks are observed, are included in Fig. 3. Although the three peaks are clearly differentiated, a deconvolution of the TPR patterns has been performed in order to identify the area that correspond to each peak (see also Table 2). The first peak appears between 50 and 112 °C and is assigned to the PdO reduction to metallic Pd [35,37,46,70]. This peak is better defined and occurs at a lower temperature in the samples that present a higher percentage of Pd (see Table 2). Some authors have related the amount of Pd in the catalyst with the crystallite size and the type of interaction between the support and the metal [46]. By increasing the palladium content, the appearance of large Pd particles is favored, which are reduced at low temperatures. However, in the samples that have a lower percentage of palladium, the palladium is found in the form of smaller dispersed species whose interaction with the support is greater. In the two samples in which the Pd content is higher (0.36 and 0.46 wt%), a negative TPR peak was observed, which was attributed to the decomposition of the Pd hydride (β-PdH_2) formed at room temperature from the absorption of atomic hydrogen within the structure of large size metallic Pd particles. That is, in these two samples a decrease in the baseline is observed as a consequence of an increase in the hydrogen that reaches the TCD detector [43,71–73]. Therefore, for the bimetallic samples, the absence of the hydride phase may indicate a good dispersion of Pd, staying in interaction with the second metal [43]. The second peak that can be observed in all Ni-Pd/Al_2O_3 TPR patterns appears between 430 and 442 °C. This peak is caused by the reduction of NiO species to Ni [26,35,37,46,65,70]. Finally, between 766 and 787 °C there is a peak that is generated by the reduction of the $NiAl_2O_4$ species and the structural and phase changes that occur above the calcination temperature [37,70]. Some authors have suggested that Ni-Pd/Al_2O_3 catalysts are reduced more convenient than Ni/Al_2O_3 catalysts due to the promotion with the noble metal, which is consistent with what was observed in these patterns [35–37,39,46]. Previous studies have related the presence of Pd particles with the reduction or disappearance of the $NiAl_2O_4$ spinel [37,39,46]. These studies have made their Ni-Pd/Al_2O_3 catalysts by co-impregnation of both metals on the same γ-Al_2O_3 support. However, in this serie, nickel impregnation was performed first, followed by palladium impregnation. In this way, the spinel had already formed and the addition of palladium did not affect it.

As reflected in the data presented in Table 2, by adding Pd to the catalysts, the area of the α-type NiO reduction peak increases significantly. However, as occurs with molybdenum, in the samples with 0.36 and 0.46 wt% Pd, this upward trend is not observed. It is likely that this change in trend observed in the samples with higher wt.% of Pd is due to the decrease in the baseline generated by the decomposition of the Pd hydride.

If we compare the results from Ni-Mo and Ni-Pd, it is observed that palladium favors the appearance of NiO species with a lower interaction with the support. In this very line, Mihet *et al.* [37] reported that promotion with Rh favors to a greater extent the formation of NiO weakly interacting with the alumina support compared to the Ni–Pd/Al_2O_3 catalyst. Although the promotion with molybdenum generates NiO species whose interaction with the support is higher, the TPR results of both bimetallic catalysts suggest a close proximity of the two metals, which increases the reducibility of the catalyst [39,74]. Therefore, the nickel oxide nanoparticle would be activated easier to provide active nickel sites.

As explained above, a Ni-Mo-Pd/Al_2O_3 catalyst has been generated by adding palladium to the Ni(10 %)-Mo(8.6 %)/Al_2O_3 catalyst until reaching 0.13 wt% of Pd (Ni(10 %)-Mo(8.6 %)-Pd(0.13 %)/Al_2O_3). In the case of the Ni-Pd-Mo/Al_2O_3 catalyst, the catalyst that was impregnated with molybdenum until obtaining 8.6 wt% of this metal was Ni

Table 2
Maximum temperature and the areas of the peaks obtained after the deconvolution of the TPR curves of Ni(10%)/Al_2O_3 and Ni(10%)-Pd(Y%)/Al_2O_3 catalyst.

Catalyst	PdO		α-NiO		β_1-NiO		$NiAl_2O_4$	
	T max (°C)	Peak area [a.u.]	T max (°C)	Peak area [a.u.]	T max (°C)	Peak area [a.u.]	T max (°C)	Peak area [a.u.]
Ni(10 %)/ Al_2O_3	–	–	335	0.8	556	2.9	756	14.2
Ni(10 %)-Pd(0.07 %)/Al_2O_3	112	0.6	434	1.2	–	–	766	7.8
Ni(10 %)-Pd(0.13 %)/Al_2O_3	99	1.4	434	2	–	–	773	6.7
Ni(10 %)-Pd(0.19 %)/Al_2O_3	76	1.2	430	1.8	–	–	776	6.9
Ni(10 %)-Pd(0.36 %)/Al_2O_3	53	1.7	440	0.5	–	–	785	5.5
Ni(10 %)-Pd(0.46 %)/Al_2O_3	50	1.4	442	0.4	–	–	787	5.8

(10 %)-Pd(0.13 %)/Al_2O_3 (Ni(10 %)-Pd(0.13 %)-Mo(8.6 %)/Al_2O_3). The TPR patterns (and the corresponding deconvolutions) of these four catalysts, as well as the initial Ni/Al_2O_3 sample are included in Fig. 4. The maximum temperatures and the the areas of the peaks present in the TPR curves of these samples are summarized in Table 3. In both samples the same five peaks that appear at very similar temperatures can be observed. First of all, the PdO reduction peak that was detected in the Ni-Pd samples can be observed at a temperature of 99 °C [35,37,46,70]. Between 445 and 455 °C a peak corresponding to the α-type NiO species appears, species with a weak interaction with the support [26,35,46,65]. Around 600 °C, in both samples a high intensity peak is observed whose area is around 30–40. This peak is generated as a consequence of the simultaneous reduction of β_1-type NiO, MoO_3, and $NiMoO_4$ [26,32,69]. As can be seen in Fig. 4, this reduction peak appears at the same temperature in these two trimetallic catalysts and in the Ni-Mo catalyst. As mentioned in the characterization of bimetallic catalysts, between 756 and 772 °C the reduction of $NiAl_2O_4$ and MoO_2 to Mo generates an easily identifiable peak [26,68,69]. Finally, between 927 and 952 °C, a

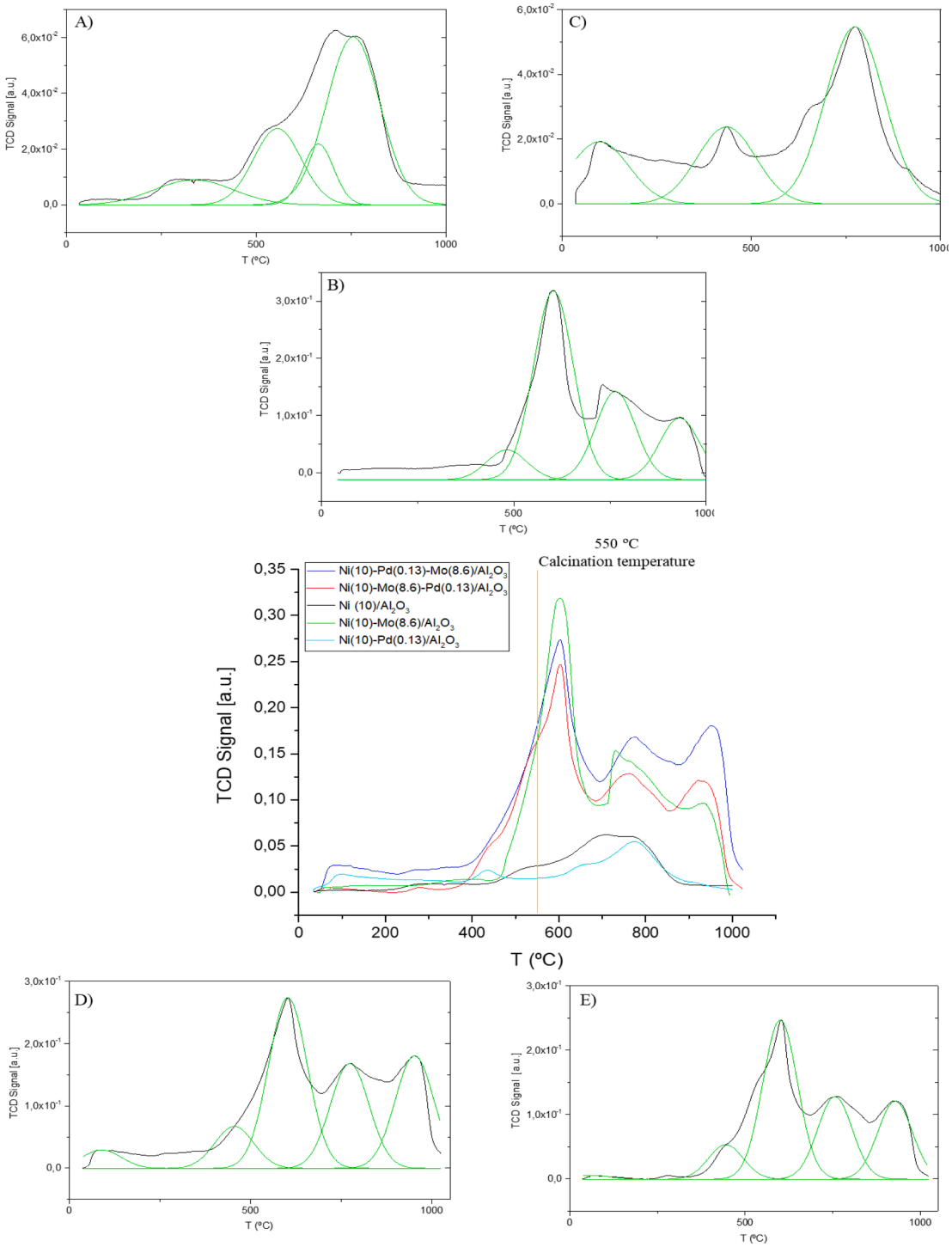

Fig. 4. TPR patterns of Ni-Mo-Pd/Al_2O_3 samples. All catalysts were previously calcined at 550 °C. Peak deconvolution of: A) Ni(10 %)/Al_2O_3; B) Ni(10 %)-Mo(8.6 %)/Al_2O_3; C) Ni(10 %)-Pd(0.13 %)/Al_2O_3; D) Ni(10 %)-Pd(0.13 %)-Mo(8.6 %)/Al_2O_3; E) Ni(10 %)-Mo(8.6 %)-Pd(0.13 %)/Al_2O_3. The TPR patterns comparison is included in the central Figure.

Table 3
Maximum temperature and the areas of the peaks obtained after the deconvolution of the TPR curves of Ni(10%)/Al_2O_3, Ni(10%)-Mo(8.6%)/Al_2O_3, Ni(10%)-Pd (0.13%)/Al_2O_3, Ni(10%)-Mo(8.6%)-Pd(0.13%)/Al_2O_3 and Ni(10%)-Pd(0.13%)-Mo(8.6%)/Al_2O_3 catalysts.

Catalyst	PdO		α-NiO		β_1-NiO/MoO_3/$NiMoO_4$		MoO_2/$NiAl_2O_4$		$Al_2(MoO_4)_3$	
	T max (°C)	Peak area [a.u.]	T max (°C)	Peak area [a.u.]	T max (°C)	Peak area [a.u.]	T max (°C)	Peak area [a.u.]	T max (°C)	Peak area [a.u.]
Ni(10 %)/Al_2O_3	–	–	335	0.8	556	2.9	756	14.2	–	–
Ni(10 %)-Mo(8.6 %)/Al_2O_3	–	–	482	6.6	603	42.9	764	20	931	14.1
Ni(10 %)-Pd(0.13 %)/Al_2O_3	99	1.4	434	2	–	–	773	6.7	–	–
Ni(10 %)-Mo(8.6 %)-Pd(0.13 %)/Al_2O_3	63	0.5	439	6.3	602	30.9	756	16	927	14.7
Ni(10 %)-Pd(0.13 %)-Mo(8.6 %)/Al_2O_3	76	0.8	447	8.7	603	32.2	772	18.9	952	18.8

characteristic peak of the samples containing molybdenum is observed, which is generated as a consequence of the reduction of $Al_2(MoO_4)_3$ [26,32,68].

The maximum temperatures and the areas of the reduction peaks present in the trimetallic catalysts are included in Table 3. The effects of Mo and Pd on the reducing properties of NiO are clearly observed. Around 439–447 °C, the reduction peak of the NiO species that interact slightly with the support appears, which had already been observed in

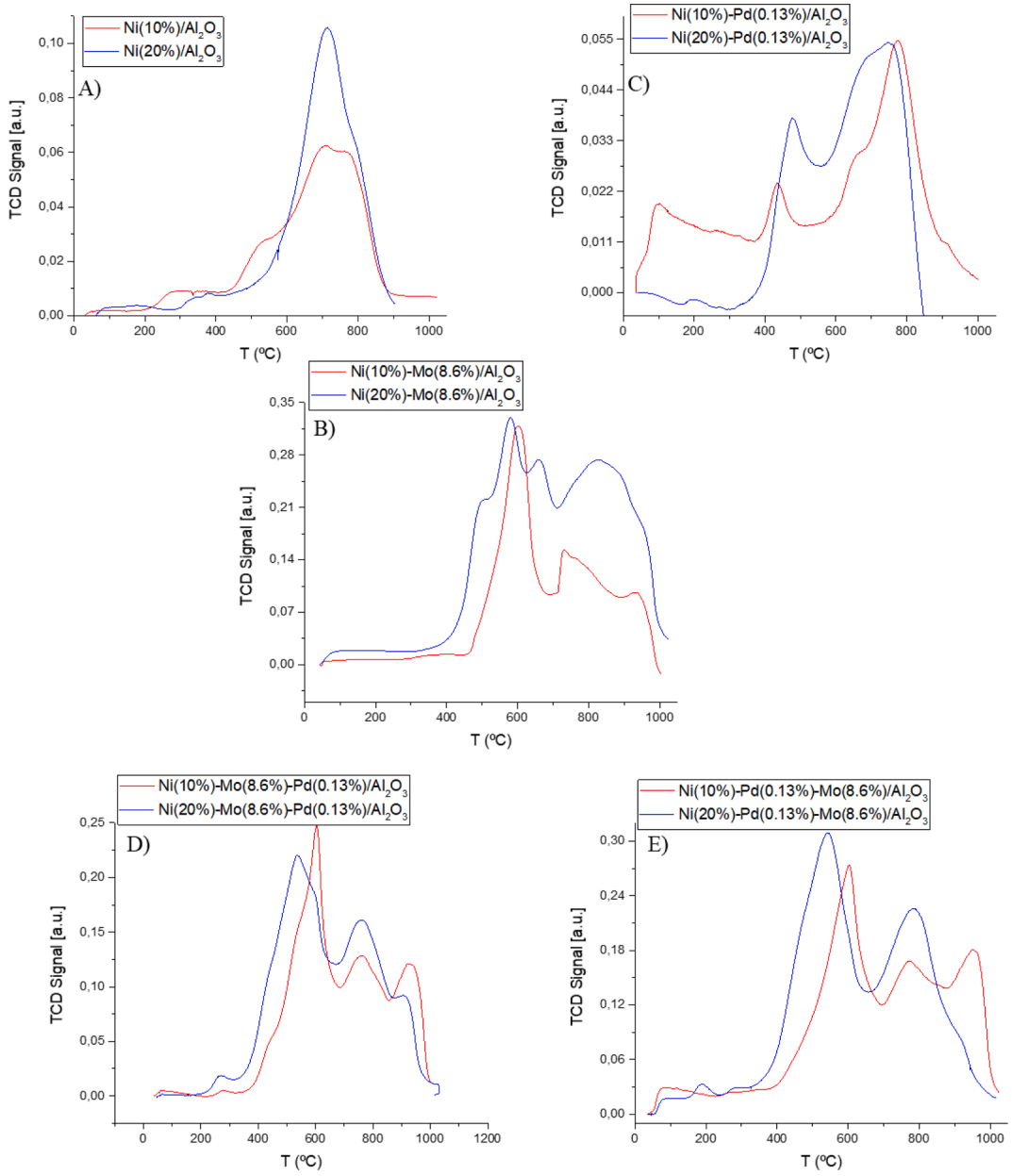

Fig. 5. Comparison of the TPR patterns of the catalysts with 10 and 20 wt% Ni: A) Ni/Al_2O_3; B) Ni-Mo(8.6%)/Al_2O_3; C) Ni-Pd(0.13%)/Al_2O_3; D) Ni-Mo(8.6%)-Pd (0.13%)/Al_2O_3; E) Ni-Pd(0.13%)-Mo(8.6%)/Al_2O_3.

the Ni-Pd catalysts. The intense peak of the β_1-type NiO species that appears in the Ni-Mo catalysts is also observed with a very similar area.

3.1.1. Effect of nickel content on catalysts

After studying the reducing properties and the species that are formed when modifying the Mo and Pd contents, catalysts with 20 wt% of Ni were prepared to check if the reduction process is affected. A comparison of the TPR curves of catalysts with 10 wt% Ni and catalysts with 20 wt% Ni is shown in Fig. 5. In Fig. 5**A** we find the reduction patterns of the monometallic samples (Ni(10 %)/Al_2O_3 and Ni(20 %)/Al_2O_3). In these samples, increasing the wt.% Ni does not improve the reducing properties of the catalyst. These data do not coincide with those obtained by Zhang *et al.* [59], who suggested that the interaction between NiO and the alumina support was weaker as the percentage of nickel increased. For these authors, the reduction of the interaction is due to the fact that in the samples with a greater amount of nickel, the crystal size of the Ni particles is greater. In the TPR patterns of the bimetallic catalysts containing nickel and 8.6 wt% Mo (Ni(10 %)-Mo (8.6 %)/Al_2O_3 and Ni(20 %)-Mo(8.6 %)/Al_2O_3, Fig. 5**B**), it is observed that in the presence of this second metal, the increase in the amount of nickel improves the reducing properties of the catalyst. First of all, the interaction between both metals causes the highest intensity peak of the pattern to shift downwards with increasing Ni content (603–578 °C), suggesting a weaker bond of β_1-NiO with the alumina support for samples with higher Ni loading. In addition, the α-type NiO peak, which was barely intuited in the sample with 10 wt% Ni, appears with much greater intensity and is clearly differentiated in the catalyst with 20 wt% Ni. These results fully coincide with what was found by other authors, who also verified that these catalysts with a higher percentage of nickel had higher catalytic performance [33,57]. The curves presented in Fig. 5**C** suggest that in nickel-palladium bimetallic catalysts (Ni(10 %)-Pd(0.13 %)/Al_2O_3 and Ni(20 %)-Pd(0.13 %)/Al_2O_3), increasing the wt.% of Ni does not modify the type of interactions that occur between NiO and the support. That is, the interaction between these two metals is different from the interaction between Ni and Mo, so as the amount of Ni increases, the reduction temperature of NiO does not decrease. Although the α-type NiO peak is more intense in the sample with more Ni, the peaks corresponding to NiO with stronger interactions also increase in intensity. These results accord to the reported by Yongwoo *et al.* [75]. From the results included in Fig. 5**D and 5E**, it can be verified that in the trimetallic catalysts, when the wt.% Ni increases to 20, weaker interactions are formed between the NiO and the support, decreasing its reduction temperature. In the TPR curve of the Ni(20 %)-Mo-Pd/Al_2O_3 sample, it is clearly seen how the increase in wt.% Ni favors the NiO species that are reduced at 436 or 535 °C, compared to those that are reduced at 594 °C, which were the ones that present a more intense reduction peak in the sample with 10 wt% Ni. In addition, this Ni content increase has also favored the appearance of a small peak around 270 °C, which is probably caused by the reduction of NiO that has not been bound to the support [68,76]. When adding molybdenum to the catalyst with 20 wt% Ni and 0.13 wt% Pd (Fig. 5**E**), the TPR curve changes and the interaction between the support and NiO becomes weaker. Therefore, it seems that the fact that the reduction of NiO occurs at a lower temperature when the percentage of Ni increases is directly related to the presence of Mo. In according to what was observed in the Ni-Mo catalysts with 10 wt% Ni, in the samples with a higher Mo/Ni ratio, the peak corresponding to the reduction of $Al_2(MoO_4)_3$ is more intense. This suggests that the lower this ratio, the lower the interaction between the metals and the support. In addition, in the two trimetallic samples and in the Ni-Pd sample that have 20 wt% of Ni, a decrease in the intensity of the PdO reduction peak that appears at 85 °C is observed, which suggests a greater dispersion of palladium with increasing Ni content. As previously mentioned, the small palladium particles that are well dispersed throughout the support have a higher reduction temperature [46]. According to Soszka *et al.* and Yongwoo *et al.*, the PdO peak is highly dependent on the Ni/Pd ratio of the catalysts, being higher when this ratio is lower [46,75].

3.1.2. Effect of impregnation order

A comparison of nickel palladium and nickel molibdenum bimetallic catalysts impregnated in different order is summarized in Fig. 6 (Ni(10 %)-Mo(8.6 %)/Al_2O_3 vs Mo(8.6 %)-Ni(10 %)/Al_2O_3 and Ni(10 %)-Pd (0.13 %)/Al_2O_3 vs Pd(0.13 %)-Ni(10 %)/Al_2O_3). From the results included in Fig. 6**A** it is evident that impregnating the Mo first significantly improves the catalyst, shifting the NiO reduction peaks to the left and making them much more intense. The α-type NiO peak shift from 482 to 477 °C, while the β_1-type NiO peak shift from 603 to 571 °C. Basha *et al.* [77] impregnated Ni and Mo on a non-alumina support and showed that impregnating nickel first improved the catalyst properties and increased its performance. This difference is due to the type of support used, since Al_2O_3 was not used, $NiAl_2O_4$ was not formed. The reduction patterns of the two catalysts containing Ni and Pd is summarized in Fig. 6**B**. This graph shows that the order of impregnation of Ni and Pd also has a significant effect on the type of interactions that are formed in the catalyst. By impregnating Pd first (Pd(0.13 %)-Ni(10 %)/Al_2O_3), the $NiAl_2O_4$ peak practically disappears, while the α-type NiO peak (434 °C) and especially the peak of the NiO species that have a stronger interaction with it (650 °C) appear with a greater intensity. In addition, the TPR curve of this Pd-Ni catalyst is more similar to Ni-Pd catalysts with a higher wt.% Pd, since a decrease from the baseline to negative values caused by the decomposition of Pd hydride is observed [43,71–73]. Therefore, it seems that the order of impregnation is a crucial factor in reducing the formation of the $NiAl_2O_4$ spinel, which is not active.

3.2. Temperature-Programmed reduction analysis of samples generated by co-impregnation

A comparison of the two bimetallic catalysts (Ni(10 %)-Mo(8.6 %)/Al_2O_3 vs [Ni(10 %)-Mo(8.6 %)]/Al_2O_3 and Ni(10 %)-Pd(0.13 %)/Al_2O_3 vs [Ni(10 %)-Pd(0.13 %)]/Al_2O_3) and the two trimetallic catalysts prepared by individual sequential impregnations versus the catalysts prepared by co-impregnation (Ni(10 %)-Mo(8.6 %)-Pd(0.13 %)/Al_2O_3 vs [Ni(10 %)-Mo(8.6 %)]-Pd(0.13 %)/Al_2O_3 and Ni(10 %)-Pd (0.13 %)-Mo(8.6 %)/Al_2O_3 vs [Ni(10 %)-Pd(0.13 %)]-Mo(8.6 %)/Al_2O_3) is summarized in Fig. 7. From these results, it is clear that the interactions are different depending on the preparation method. That is, the way of impregnating the metals affects the metal–metal and metal-support interaction. A comparison between the two samples with Ni-Pd and Ni(10 %)/Al_2O_3 is presented in Fig. 7**A**. The peak that appears around 435 °C, caused by the reduction of α-type NiO species that have a weak interaction with the support, is much more intense in the sample generated by co-impregnation. In addition, at a temperature of 547 °C, the peak corresponding to more difficultly reducible NiO species appears, which is not observed in the curve of the sample generated by sequential impregnations. The results indicate that when palladium and nickel are impregnated together, there is an interaction between the two metals that favors the formation of more easily reducible NiO species, which would possibly increase the performance of the catalyst. That is, in both the monometallic catalyst and the bimetallic catalyst obtained by sequential impregnation, most of the nickel seems to be in the form of $NiAl_2O_4$, which does not occur when co-impregnating the two metals. Other authors have previously reported the reduction of the interaction with the support of Ni particles when adding palladium to their catalysts [35,37,39,46,70]. However, the important effect that the preparation method has on the catalyst reducibility has not been described. The fact that the addition of small amounts of Pd with Ni increase the reducibility of the catalyst suggests a close proximity of the metals in the catalyst structure [74]. Palladium is a good hydrogen dissociation site, therefore, this dissociated hydrogen migrates across the catalyst surface reducing NiO more easily than molecular H_2 present in the gas pase The PdO peak is not seen in the sample obtained by co-impregnation.

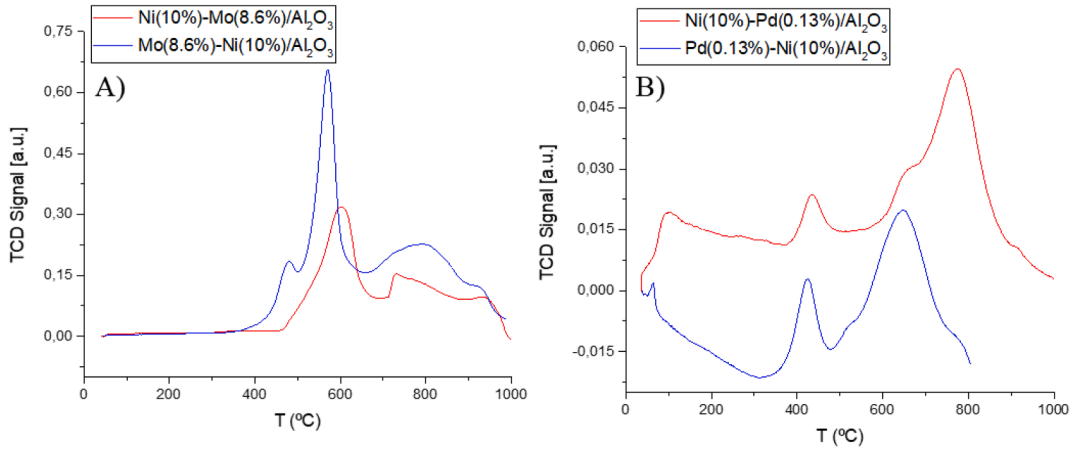

Fig. 6. Differences in the TPR patterns depending on the order of Ni impregnation. A) Ni(10%)-Pd(0.13%)/Al_2O_3 vs Pd(0.13%)-Ni(10%)/Al_2O_3; B) Ni(10%)-Mo(8.6%)/Al_2O_3 vs Mo(8.6%)-Ni(10%)/Al_2O_3.

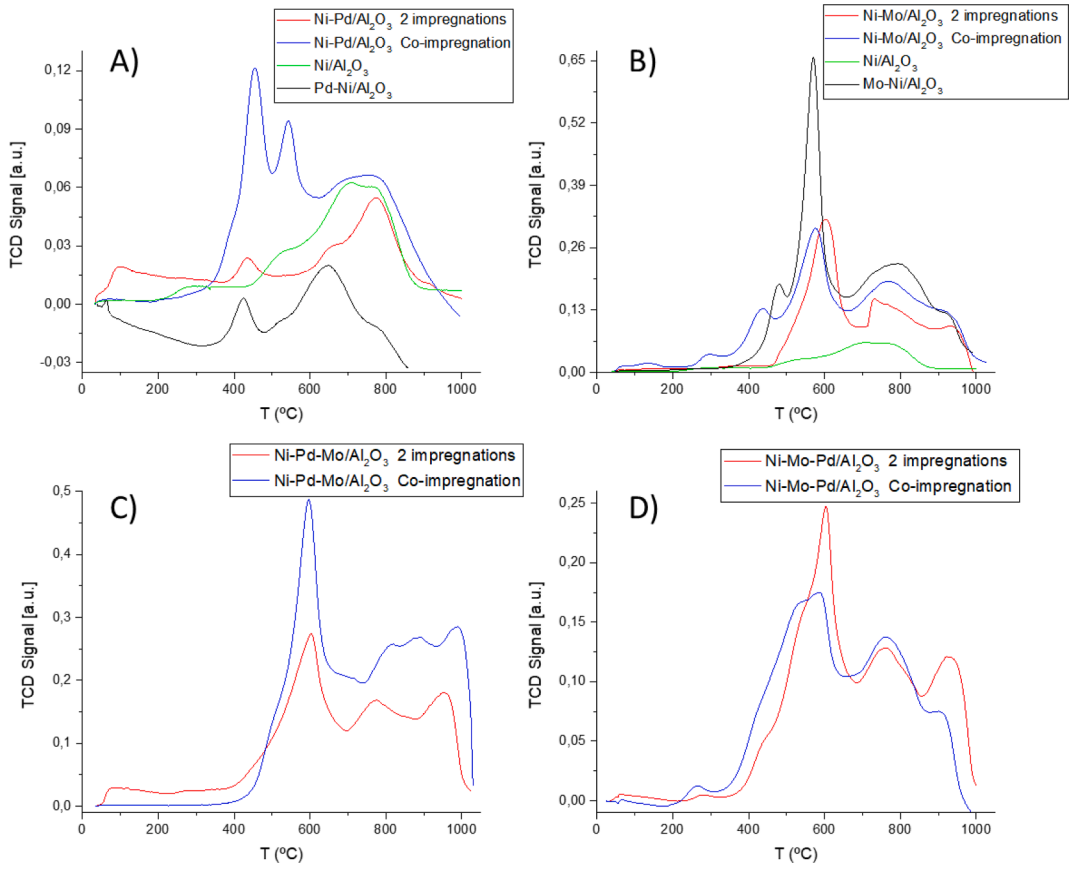

Fig. 7. Comparison of the TPR patterns of catalysts prepared by co-impregnation and those prepared by sequential impregnation. A) Ni(10%)-Pd(0.13%)/Al_2O_3; B) Ni(10%)-Mo(8.6%)/Al_2O_3; C) Ni(10%)-Pd(0.13%)-Mo(8.6%)/Al_2O_3; D) Ni(10%)-Mo(8.6%)-Pd(0.13%)/Al_2O_3.

A comparison between the two samples with Ni-Mo and Ni(10 %)/Al_2O_3 is presented in Fig. 7**B**. As in the Ni-Pd catalysts, a significant difference is observed between the catalyst generated by sequential impregnations and the one synthesized by co-impregnation of Ni and Mo. The highest intensity peak, which is caused in part by the reduction of β_1-type NiO species, shifts to a lower temperature by impregnating the metals together, approaching the temperature at which this peak appears in the monometallic sample. In the TPR curve of the co-impregnated sample, two new peaks appear around 300 and 430 °C. The small peak at 300 °C was reported on the reduction of unbounded free NiO [68,76], while the peak observed at 430 °C is generated by the reduction of NiO that does have a weak interaction with the support [17,32,33]. This peak of the α-type NiO species appears with a much higher intensity in the bimetallic catalyst synthesized by co-impregnation than in Ni/Al_2O_3, which coincides with that described by other authors [20,68]. This means that, as with Pd, adding Ni and Mo together favors a weaker interaction between nickel and the support and improves the properties of the catalyst. In addition, in accord to what was observed in the other bimetallic catalyst, the data suggest that in Ni-Mo/Al_2O_3 catalysts the type of impregnation notably modifies the

characteristics of the catalyst such as reducibility or the metal oxides that are formed. Therefore, unlike the Ni-Pd catalyst, although co-impregnation of Ni and Mo decreases the interaction between the metals and the support, it seems that sequential impregnation of the metals by first adding Mo could give good results too.

Two comparisons of trimetallic catalysts generated by sequential impregnation and those generated by co-impregnation are shown in Fig. 7**C** and Fig. 7**D**. Following the trend observed in bimetallic catalysts, when Ni and Pd are impregnated together, the appearance of NiO species is favored over $NiAl_2O_4$, while when Ni and Mo are impregnated together, the reduction temperature of these NiO species decreases.

As a general conclusion, it can be said that the reduction properties are better observed in the catalysts prepared by co-impregnation than in those prepared by sequential impregnation. There are several studies that defend that sequential impregnation can give better results than co-impregnation [4,75,78]. However, in none of these studies has nickel been impregnated on alumina, so $NiAl_2O_4$ is not formed in their catalysts. Probably, the reason why co-impregnation gives better results in our catalysts is because the formation of spinel-like $NiAl_2O_4$ is reduced, favoring the formation of NiO particles that interact slightly with the support and are more easily reducible. According to the results found by Crisafulli *et al.* [79], co-impregnation of Pd and Ni on a SiO_2 support does not show a significant change in the reduction peaks compared to the peaks observed in the monometallic catalysts. This reinforces our hypothesis, since in the silica support nickel does not form spinel-type structures and in monometallic catalysts all Ni is already present as NiO. In the same way, there are also some authors who have obtained results more in line with ours and claim to have obtained better results

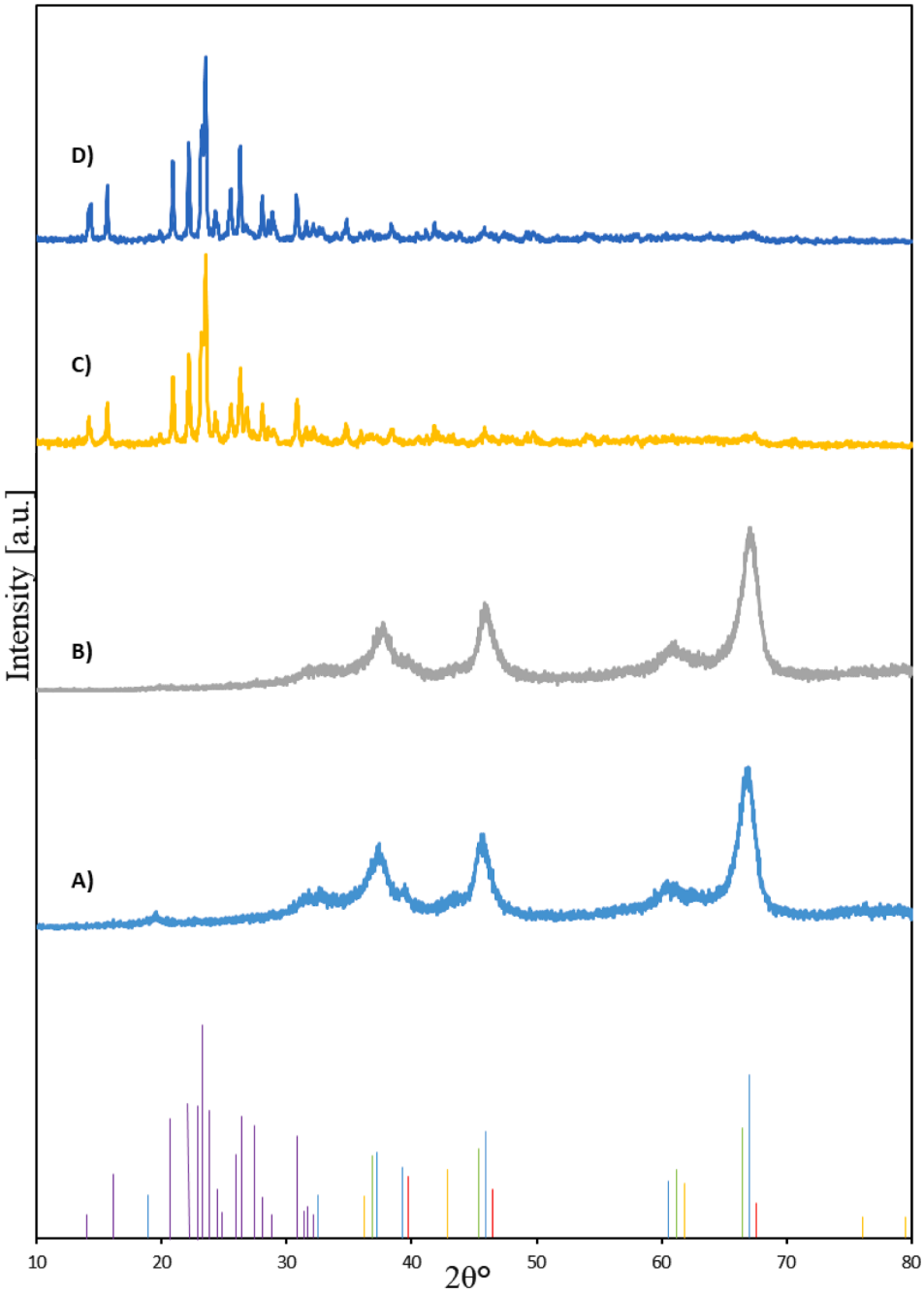

Fig. 8. XRD patterns of: A) Ni(10%)/Al_2O_3; B) Ni(10%)-Pd(0.13%)/Al_2O_3; C) Ni(10%)-Mo(8.6%)/Al_2O_3; D) Ni(10%)-Mo(8.6%)-Pd(0.13%)/Al_2O_3. Al_2O_3 - ICDD card, File 00-010-0425; Pd - ICDD card, File 00–046-1043; $NiAl_2O_4$ - ICDD card, File 00-001-1299; NiO - ICDD card, File 01-073-1519.

through the co-impregnation procedure [80–82].

3.3. Powder XRD

The XRD technique was used to explain the crystal morphology and the presence of Ni, Mo and Pd on the Al_2O_3 support. XRD runs recorded at a 2θ angular range of $10 - 80^\circ$ are shown in Fig. 8. In addition, in order to confirm what was observed by TPR, The evolution of the NiO diffraction peaks as a function of the impregnation method and the wt.% Ni are summarized in Figs. 9 and 10. The peaks of the metals were observed in their oxide phases, before carrying out any type of reduction. The intensity of the peaks represents the crystallinity of the catalysts. Sharper peaks means particles tend to get higher crystallinity. High crystallinity will affect catalytic activity and stability at higher temperature [19].

The diffraction patterns of the Ni(10 %)/Al_2O_3 catalyst, two bimetallic catalysts (Ni(10 %)-Pd(0.13 %)/Al_2O_3 and Ni(10 %)-Mo(8.6 %)/Al_2O_3) and one trimetallic catalyst (Ni(10 %)-Mo(8.6 %)-Pd(0.13 %)/Al_2O_3) after being calcined at 550 °C for 4 h were included in Fig. 8. At the bottom of Fig. 8 it can be seen the four main diffraction patterns that have been detected in these simples. In all samples, but specially in the patterns of the monometallic catalyst and Ni(10 %)-Pd(0.13 %)/Al_2O_3 catalyst, seven diffraction peaks are clearly visible at $2\theta =$ 19.45, 31.93, 37.60, 39.49, 45.86, 60.89 and 67.03°. These peaks correspond to the typical cubic structure of aluminum oxide (ICDD card, File No. 00–010-0425). Furthermore, these data agree with the characterization of pure γ-Al_2O_3 that showed the diffraction peaks at $2\theta =$ 37, 40, 46, and 67° [56,83]. In the samples containing molybdenum, MoO_3 diffraction peaks appeared at 2θ of 20.95, 23.17, 23.32, 23.56 and 26.31 [26,29,84]. In addition, in both patterns the characteristic peaks of the orthorhombic cristal structure of $Al_2(MoO_4)_3$ are clearly observed (ICDD card, File No. 00–023-0764). In the XRD patterns of the Ni(10 %)-Pd(0.13 %)/Al_2O_3 and Ni(10 %)-Mo(8.6 %)-Pd(0.13 %)/Al_2O_3 samples, peaks have been detected at 2θ of 39.12, 46.66 and 68.12, which coincide with the cubic structure of Pd (ICDD card, File 00–046-1043). However, these peaks are overlapped with the peaks of the support and correspond to structures with low crystallinity, so they are not appreciated. Finally, the presence of XRD patterns that correspond to the cubic structures of nickel oxide (ICDD card, File No. 001–073-1519) and nickel aluminum oxide (ICDD card, File 00–001-1299) have been detected in all samples, even though the peaks corresponding to these patterns are difficult to distinguish from the γ-Al_2O_3 peaks due to overlapping of the peaks [26,29]. The peak of greatest intensity of this cubic structure of NiO ($2\theta = 43.38^\circ$) is the one that is best appreciated without any overlapping [85]. In addition, as other authors have reported, probably there are NiO species in the amorphous pase or

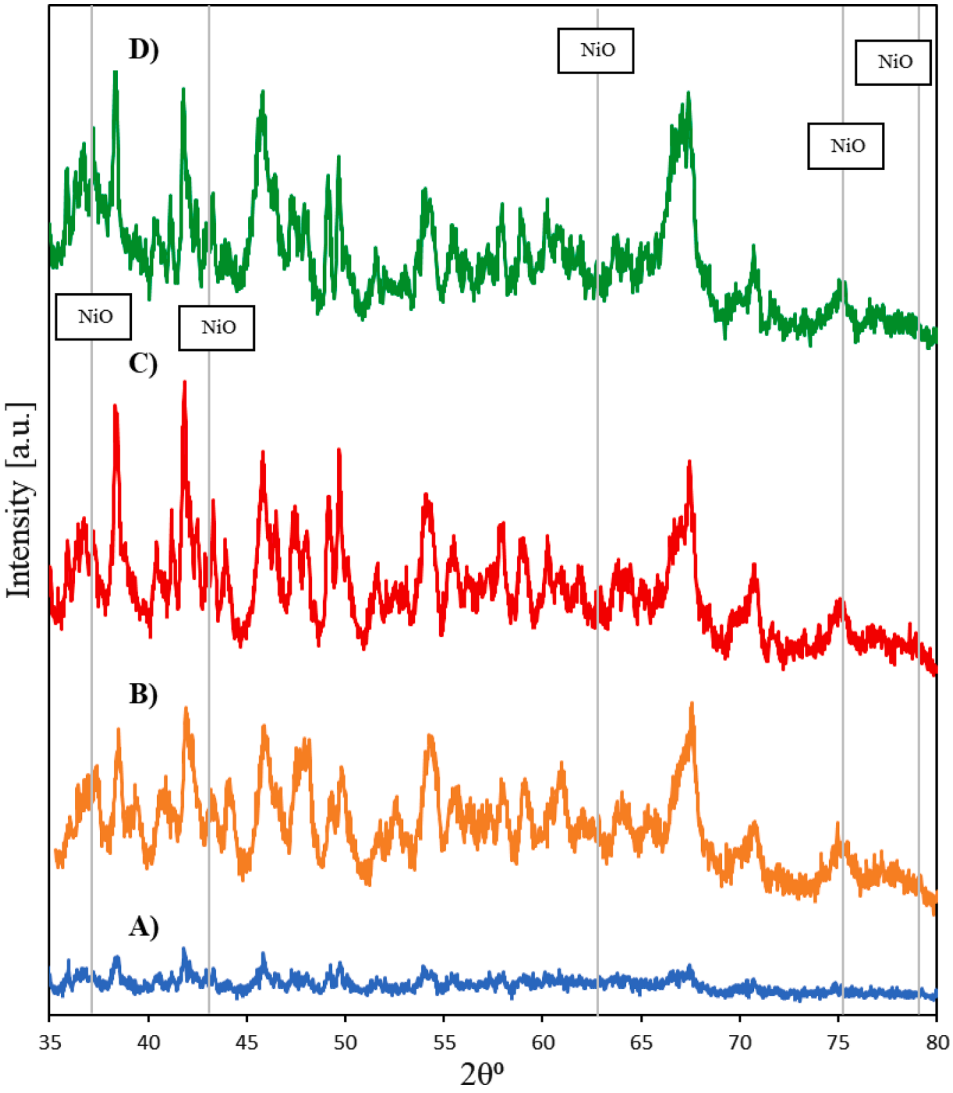

Fig. 9. XRD patterns of 4 different nickel molybdenum catalysts: A) Ni(10%)-Mo(8.6%)/Al_2O_3. B) Mo(8.6%)-Ni(10%)/Al_2O_3. C) Ni(20%)-Mo(8.6%)/Al_2O_3. D) [Ni(10%)-Mo(8.6%)]/Al_2O_3. NiO - ICDD card, File 01-073-1519.

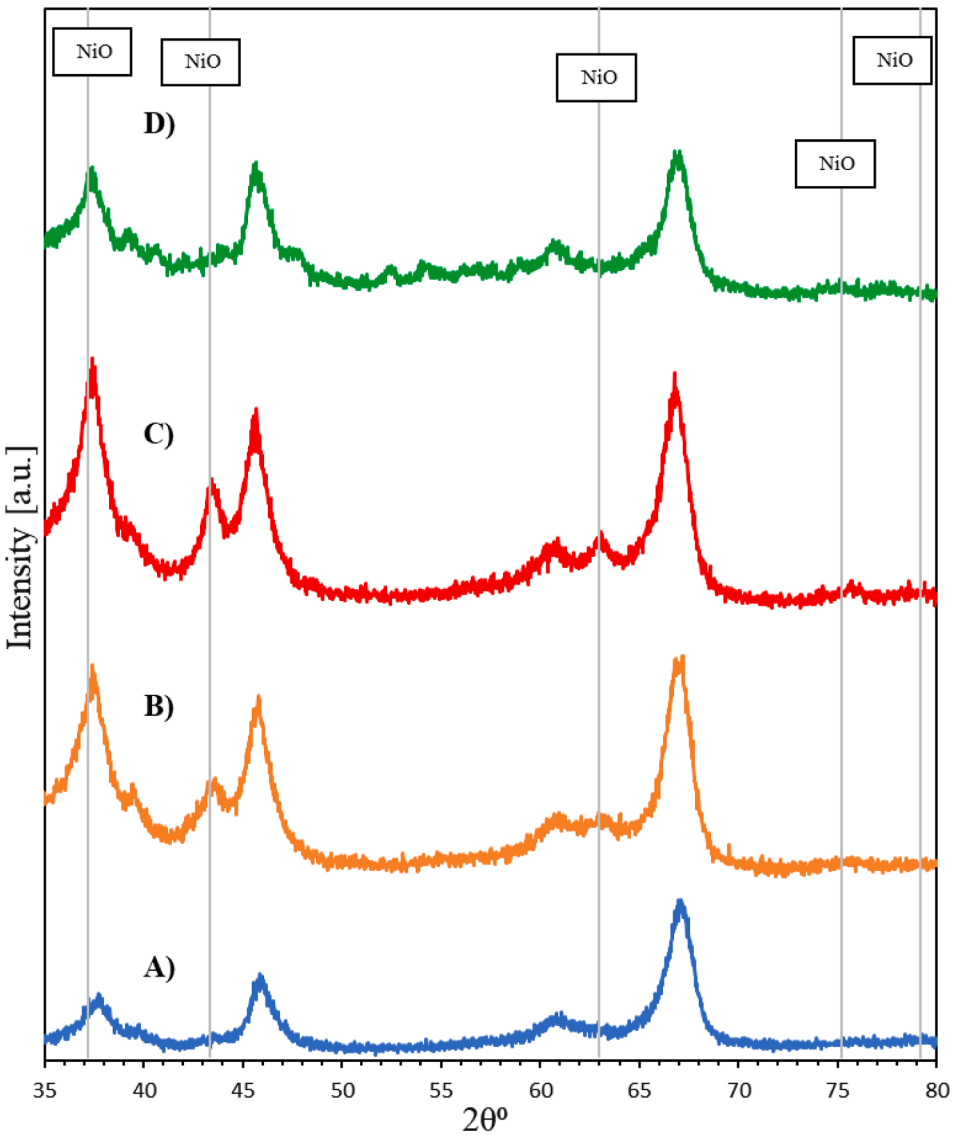

Fig. 10. XRD patterns of 4 different nickel molybdenum catalysts: A) Ni(10%)-Pd(0.13%)/Al_2O_3. B) Pd(0.13%)-Ni(10%)/Al_2O_3. C) Ni(20%)-Pd(0.13%)/Al_2O_3. D) [Ni(10%)-Pd(0.13%)]/Al_2O_3. NiO - ICDD card, File 01-073-1519.

microcrystallines, which are too little to be discovered by XRD [29,33]. It is possible that the nickel oxide is highly dispersed over the alumina, which can make it difficult to visualize by XRD analysis [17].

The diffraction patterns of three bimetallic catalysts that were impregnated in different ways and one catalyst whose Ni wt.% is 20 instead of 10 are included in Figs. 9 and 10. In both figures it is observed that in the samples with 20 wt% Ni (XRD 9C and 10C) the intensity of the diffraction peaks of NiO is greater (especially the peaks that appear at 2θ of 37 and 43°). In addition, as can be seen in XRD B and D of the figures, both when Ni is impregnated second and when both metals are co-impregnated at the same time, the intensity of the NiO peaks also increases, as well as the sample crystallinity. These data agree with what was observed by TPR, that is, both the co-impregnation and the initial impregnation of Pd or Mo favor Ni to be found as NiO, compared to other forms such as spinel-like $NiAl_2O_4$, which is not active.

4. Conclusions

The following conclusions can be derived from the results of the present work:

a) In the bimetallic Ni-Mo catalysts supported on alumina, the samples with a higher Ni/Mo ratio present a weaker interaction of both metals with the support. In addition, the interaction between Mo and Ni favors the appearance of more reducible NiO species than the interaction between Ni and Mo.
b) The order of impregnation of Mo and Pd does not seem to affect the reducing properties of the Ni-Mo-Pd trimetallic catalysts generated by sequential impregnation, since both catalysts presented very similar TPR patterns, with peaks in the same positions.
c) Increasing the Ni/Pd ratio of bimetallic catalysts does not affect the reduction temperature of NiO, but it facilitates the distribution of Pd in the form of small, well dispersed particles that are reduced at low temperature.
d) When synthesizing catalysts by the sequential impregnation method, the Ni impregnation order is a determining factor. If Ni is impregnated second, this metal is distributed in the form of NiO in a greater proportion than if it is impregnated first.
e) The preparation method greatly affects the reducing properties of the catalysts. The initial co-impregnation of Ni with another metal hinders the appearance of spinel-like $NiAl_2O_4$, favoring nickel to be added in the form of more easily reducible NiO particles. Therefore,

in alumina-supported Ni catalysts, co-impregnation is a method that gives better results than sequential impregnation. Even so, in molybdenum containing catalysts, the previous individual impregnation of molybdenum also significantly improves the properties of the catalyst, equaling or exceeding those of the co-impregnated.

f) The programmed-temperature reduction technique is used to characterize the reduction capacity of the metal oxides present in the catalyst. In future research, it is necessary to check the effect that these changes in the reducing properties have on the performance of the catalysts.

CRediT authorship contribution statement

Ivan Pedroarena: Investigation, Formal analysis, Writing – original draft. **Lucía Grande:** Investigation, Writing – original draft. **Jonathan J. Torrez-Herera:** Investigation, Validation, Formal analysis. **Sophia A. Korili:** Resources, Supervision. **Antonio Gil:** Resources, Funding acquisition, Conceptualization, Supervision, Writing – original draft, Methodology, Validation, Writing – review & editing.

Declaration of Competing Interest

The authors declare that they have no known competing financial interests or personal relationships that could have appeared to influence the work reported in this paper.

Data availability

No data was used for the research described in the article.

Acknowledgments

The authors are grateful for financial support from the Spanish Ministry of Science and Innovation (AEI/MINECO) and the Government of Navarra through projects PID2020-112656RB-C21 and PC034-035 BIOGASOLANA. Open access funding provided by Universidad Pública de Navarra. JJTH thanks Universidad Pública de Navarra for a post-doctoral grant. AG also thanks Santander Bank for funding via the Research Intensification Program.

References

[1] Hsu PJ, Lin YC. Hydrodeoxygenation of 4-methylguaiacol over silica-supported nickel phosphide catalysts: The particle size effect. J Taiwan Inst Chem Eng 2017; 79:80–7. https://doi.org/10.1016/j.jtice.2017.02.020.

[2] Jongerius AL, Jastrzebski R, Bruijnincx PCA, Weckhuysen BM. CoMo sulfide-catalyzed hydrodeoxygenation of lignin model compounds: An extended reaction network for the conversion of monomeric and dimeric substrates. J Catal 2012; 285:315–23. https://doi.org/10.1016/j.jcat.2011.10.006.

[3] Rinaldi N, Yoshioka M, Kubota T, Okamoto Y. Hydrodesulfurization activity of Co-Mo/Al_2O_3 catalysts prepared with citric acid: Post-treatment of calcined catalysts with high Mo loading. J Japan Pet Inst 2010;53:292–302. https://doi.org/10.1627/jpi.53.292.

[4] Nugrahaningtyas KD, Hidayat Y, Patiha N, Prihastuti B, Yelvi RUNK. Synthesis of the supported catalysts by co- impregnation and sequential impregnation methods, IOP Conf. Ser Mater Sci Eng 2017;176. https://doi.org/10.1088/1742-6596/755/1/011001.

[5] Aguilhon J, Boissière C, Durupthy O, Thomazeau C, Sanchez C. Nickel nanoparticles with controlled morphologies application in selective hydrogenation catalysis. Stud Surf Sci Catal 2020;175:521–4. https://doi.org/10.1016/S0167-2991(10)75099-0.

[6] Leu F-C, Chang T-H. Characterization of supported nickel catalysts using thermomagnetometry and TPR. J Chinese Inst Chem Eng 1996;27:121–7.

[7] Foo SY, Cheng CK, Nguyen TH, Adesina AA. Kinetic study of methane CO_2 reforming on Co-Ni/Al_2O_3 and Ce-Co-Ni/Al_2O_3 catalysts. Catal Today 2011;164: 221–6. https://doi.org/10.1016/j.cattod.2010.10.092.

[8] Wang C, Sun N, Kang M, Wen X, Zhao N, Xiao F, et al. The bifunctional mechanism of CH_4 dry reforming over Ni-Cao-ZrO_2 catalyst: further evidence via the identification of the active sites and kinetic studies, Catal. Sci Technol 2013;3: 2435–43. https://doi.org/10.1039/C3CY00153A.

[9] Zhang J, Wang H, Dalai AK. Effects of metal content on activity and stability of Ni-Co bimetallic catalysts for CO_2 reforming of CH_4. Appl Catal A Gener 2008;339: 121–9. https://doi.org/10.1016/j.apcata.2008.01.027.

[10] Pompeo F, Nichio NN, Souza MMVM, Cesar DV, Ferretti OA, Schmal M. Study of Ni and Pt catalysts supported on α-Al_2O_3 and ZrO_2 applied in methane reforming with CO_2. Appl Catal A Gener 2007;316:175–83. https://doi.org/10.1016/j.apcata.2006.09.007.

[11] Zhao X, Li H, Zhang J, Shi L, Zhang D. Design and synthesis of NiCe@m-SiO_2 yolk-shell framework catalysts with improved coke- and sintering-resistance in dry reforming of methane. Int J Hydrogen Energy 2016;41:2447–56. https://doi.org/10.1016/j.ijhydene.2015.10.111.

[12] Chang J-S, Park S-E, Lee K-W, Choi MJ. Catalytic reforming of methane with carbon dioxide over pentasil zeolite-supported nickel catalyst. Stud Surf Sci Catal 1994;84:1587–94. https://doi.org/10.1016/S0167-2991(08)63707-6.

[13] Menegazzo F, Signoretto M, Pinna F, Canton P, Pernicone N. Optimixation of bimetallic dry reforming catalysts by temperature porgrammed reaction. Appl Catal A Gener 2012;439–440:80–7. https://doi.org/10.1016/j.apcata.2012.06.041.

[14] Makri MM, Vasiliades MA, Petallidou KC, Efstathiou AM. Effect of support composition on the origin and reactivity of carbon formed during dry reforming of methane over 5 wt% Ni/$Ce_{1-x}M_xO_{2-\delta}$ ($M = Zr^{4+}$, Pr^{3+}) catalysts. Catal Today 2016; 259:150–64. https://doi.org/10.1016/j.cattod.2015.06.010.

[15] Hou Z, Gao J, Guo J, Liang D, Lou H, Zheng X. Deactivation of Ni catalysts during methane autothermal reforming with CO_2 and O_2 in a fluidized-bed reactor. J Catal 2007;250:331–41. https://doi.org/10.1016/j.jcat.2007.06.023.

[16] Yao L, Galvez ME, Hu C, Da Costa P. Mo-promoted Ni/Al_2O_3 catalyst for dry reforming of methane. Int J Hydrogen Energy 2017;42:23500–7. https://doi.org/10.1016/j.ijhydene.2017.03.208.

[17] Wang Y, Xiong G, Liu X, Yu X, Liu L, Wang J, et al. Structure and reducibility of NiO-MoO_3/γ-Al_2O_3 catalysts: Effects of loading and molar ratio. J Phys Chem C 2008;112:17265–71. https://doi.org/10.1021/jp800182j.

[18] Haider MS, Castello D, Rosendahl LA. Two-stage catalytic hydrotreatment of highly nitrogenous biocrude from continuous hydrothermal liquefaction: A rational design of the stabilization stage. Biomass Bioenergy 2020;139:105658. https://doi.org/10.1016/j.biombioe.2020.105658.

[19] Widiyadi A, Adil Guspiani G, Riady J, Andreanto R, Dea Chaiunnisa S, Widayat W, et al. Preparation and characterization of NiMo/Al_2O_3 Catalyst for Hydrocracking Processing. E3S Web Conf 2018;31:03011.

[20] Qu L, Zhang W, Kooyman PJ, Prins R. MAS NMR, TPR, and TEM studies of the interaction of NiMo with alumina and silica-alumina supports. J Catal 2003;215: 7–13. https://doi.org/10.1016/S0021-9517(02)00181-1.

[21] Haider MS, Castello D, Michalski KM, Pedersen TH, Rosendahl LA. Catalytic hydrotreatment of microalgae biocrude from continuous hydrothermal liquefaction : Heteroatom removal and their distribution in distillation cuts. Energies 2018;11:3360. https://doi.org/10.3390/en11123360.

[22] Castello D, Haider MS, Rosendahl LA. Catalytic upgrading of hydrothermal liquefaction biocrudes: Different challenges for different feedstocks. Renew Energy 2019;141:420–30. https://doi.org/10.1016/j.renene.2019.04.003.

[23] Furimsky E. Catalytic hydrodeoxygenation. Appl Catal 2000;199:147–90. https://doi.org/10.1016/S0926-860X(99)00555-4.

[24] Vrinat ML. The kinetics of the hydrodesulfurization process - a review. Appl Catal 1983;6:137–58. https://doi.org/10.1016/0166-9834(83)80260-7.

[25] Şenol OI, Viljava TR, Krause AOI. Hydrodeoxygenation of aliphatic esters on sulphided NiMo/γ-Al 2O3 and CoMo/γ-Al_2O_3 catalyst: The effect of water. Catal Today 2005;106:186–9. https://doi.org/10.1016/j.cattod.2005.07.129.

[26] Kumar P, Maity SK, Shee D. Role of NiMo alloy and Ni species in the performance of NiMo/Alumina catalysts for hydrodeoxygenation of stearic acid: A kinetic study. ACS Omega 2019;4:2833–43. https://doi.org/10.1021/acsomega.8b03592.

[27] Payen E, Grimblot J, Kasztelan S. Study of oxidic and reduced alumina-supported molybdate and heptamolybdate species by in situ laser Raman spectroscopy. J Phys Chem 1987;91:6642–8. https://doi.org/10.1021/j100311a018.

[28] Su X, An P, Gao J, Wang R, Zhang Y, Li X, et al. Selective catalytic hydrogenation of naphthalene to tetralin over a Ni-Mo/Al_2O_3 catalyst, Chinese. J Chem Eng 2020;28: 2566–76. https://doi.org/10.1016/j.cjche.2020.05.010.

[29] Liu F, Xu S, Cao L, Chi Y, Zhang T, Xue D. A comparison of NiMo/Al_2O_3 catalysts prepared by impregnation and coprecipitation methods for hydrodesulfurization of dibenzothiophene. J Phys Chem C 2007;111:7396–402. https://doi.org/10.1021/jp068482+.

[30] Templis CC, Revelas CJ, Papastylianou AA, Papayannakos NG. Phenol hydrodeoxygenation over a reduced and sulfided NiMo/γ-Al_2O_3 catalyst. Ind Eng Chem Res 2019;58:6278–87. https://doi.org/10.1021/acs.iecr.8b06465.

[31] Liu Z, Han W, Hu D, Sun S, Hu A, Wang Z, et al. Effects of Ni–Al_2O_3 interaction on NiMo/Al_2O_3 hydrodesulfurization catalysts. J Catal 2020;387:62–72. https://doi.org/10.1016/j.jcat.2020.04.008.

[32] Ameen M, Azizan MT, Ramli A, Yusup S, Alnarabiji MS. Catalytic hydrodeoxygenation of rubber seed oil over sonochemically synthesized Ni-Mo/γ-Al_2O_3 catalyst for green diesel production. Ultrason Sonochem 2019;51:90–102. https://doi.org/10.1016/j.ultsonch.2018.10.011.

[33] Aboul-Enein AA, Adel-Rahman H, Haggar AM, Awadallah AE. Simple method for synthesis of carbon nanotubes over Ni-Mo/Al_2O_3 catalyst via pyrolysis of polyethylene waste using a two-stage process. Fullerenes, Nanotubes, Carbon Nanostruct 2017;25:211–22. https://doi.org/10.1080/1536383X.2016.1277422.

[34] Martínez-Juárez K, Silva-Rodrigo R, Castillo-Mares A, Guevara-Lara A, Melo-Banda JA, Vázquez-Rodríguez A, et al. Synthesis, characterization and catalytic activity of supported NiMo catalysts. Topics Catal 2011;54:535–46. https://doi.org/10.1007/s11244-011-9618-9.

[35] Batebi D, Abedini R, Mosayebi A. Combined steam and CO_2 reforming of methane (CSCRM) over Ni–Pd/Al_2O_3 catalyst for syngas formation. Int J Hydrogen Energy 2020;45:14293–310. https://doi.org/10.1016/j.ijhydene.2020.03.137.

[36] Mihet M, Lazar MD. Methanation of CO_2 on Ni/γ-Al_2O_3: Influence of Pt, Pd or Rh promotion. Catal Today 2018;306:294–9. https://doi.org/10.1016/j.cattod.2016.12.001.

[37] Mihet M, Lazar MD. Effect of Pd and Rh promotion on Ni/Al_2O_3 for NO reduction by hydrogen for stationary applications. Chem Eng J 2014;251:310–8. https://doi.org/10.1016/j.cej.2014.04.079.

[38] Jiang Y, Li Q, Li X, Wang X, Dong S, Li J, et al. Three-dimensional network Pd-Ni/γ-Al_2O_3 catalysts for highly active catalytic hydrogenation of nitrobenzene to aniline under mild conditions. ACS Omega 2021;6:9780–90. https://doi.org/10.1021/acsomega.1c00441.

[39] Bayat N, Rezaei M, Meshkani F. Hydrogen and carbon nanofibers synthesis by methane decomposition over Ni-Pd/Al_2O_3 catalyst. Int J Hydrogen Energy 2016;41:5494–503. https://doi.org/10.1016/j.ijhydene.2016.01.134.

[40] Lai Q, Zhang C, Holles JH. Hydrodeoxygenation of guaiacol over Ni@Pd and Ni@Pt bimetallic overlayer catalysts. Appl Catal A Gener 2016;528:1–13. https://doi.org/10.1016/j.apcata.2016.09.009.

[41] Zhang Y, Liao Y, Shi G, Wang W, Su B. Preparation, characterization, and catalytic performance of Pd-Ni/AC bimetallic nano-catalysts. Green Process Synth 2020;9:760–9. https://doi.org/10.1515/gps-2020-0071.

[42] Bu Q, Lei H, Zacher AH, Wang L, Ren S, Liang J, et al. A review of catalytic hydrodeoxygenation of lignin-derived phenols from biomass pyrolysis. Bioresource Technol 2012;124:470–7. https://doi.org/10.1016/j.biortech.2012.08.089.

[43] Nag NK. A study on the formation of palladium hydride in a carbon-supported palladium catalyst. J Phys Chem B 2001;105:5945–9. https://doi.org/10.1021/jp004535q.

[44] Huang Y, Wei L, Zhao X, Cheng S, Julson J, Cao Y, et al. Upgrading pine sawdust pyrolysis oil to green biofuels by HDO over zinc-assisted Pd/C catalyst. Energy Convers Manag 2016;115:8–16. https://doi.org/10.1016/j.enconman.2016.02.049.

[45] Cheng S, Wei L, Alsowij MR, Corbin F, Julson J, Boakye E, et al. In situ hydrodeoxygenation upgrading of pine sawdust bio-oil to hydrocarbon biofuel using Pd/C catalyst. J Energy Inst 2018;91:163–71. https://doi.org/10.1016/j.joei.2017.01.004.

[46] Soszka E, Jędrzejczyk M, Kocemba I, Keller N, Ruppert AM. Ni-Pd/γ-Al_2O_3 catalysts in the hydrogenation of levulinic acid and hydroxymethylfurfural towards value added chemicals. Catalysts 2020;10:1026. https://doi.org/10.3390/catal10091026.

[47] Zhang J-W, Sun K-K, Li D-D, Deng T, Lu G-P, Cai C. Pd-Ni bimetallic nanoparticles supported on active carbon as an efficient catalyst for hydrodeoxygenation of aldehydes. Appl Catal A Gener 2019;569:190–5. https://doi.org/10.1016/j.apcata.2018.10.038.

[48] Gu J, Zhang YW, Tao F. Shape control of bimetallic nanocatalysts through well-designed colloidal chemistry approaches. Chem Soc Rev 2012;41:8050–65. https://doi.org/10.1039/c2cs35184f.

[49] Śrebowata A, Juszczyk W, Kaszkur Z, Karpiński Z. Hydrodechlorination of 1,2-dichloroethane on active carbon supported palladium-nickel catalysts. Catal Today 2007;124:28–35. https://doi.org/10.1016/j.cattod.2007.02.010.

[50] Strukul G, Gavagnin R, Pinna F, Modaferri E, Perathoner S, Centi G, et al. Use of palladium based catalysts in the hydrogenation of nitrates in drinking water: From powders to membranes. Catal Today 2000;55:139–49. https://doi.org/10.1016/S0920-5861(99)00233-3.

[51] Hurst NW, Gentry SJ, Jones A, McNicol BD. Temperature Programmed Reduction. Catal Rev 1982;24:233–309. https://doi.org/10.1080/03602458208079654.

[52] Gobara HM, Hassan SA. A comparative study of surface characteristics of nickel supported on silica gel, γ-alumina, aluminosilicate. Pet Sci Technol 2009;27:1555–71. https://doi.org/10.1080/10916460802608677.

[53] Grilc M, Likozar B, Levec J. Hydrodeoxygenation and hydrocracking of solvolysed lignocellulosic biomass by oxide, reduced and sulphide form of NiMo, Ni, Mo and Pd catalysts. Appl Catal B Environ 2014;150–151:275–87. https://doi.org/10.1016/j.apcatb.2013.12.030.

[54] Mochizuki T, Chen SY, Toba M, Yoshimura Y. Deoxygenation of guaiacol and woody tar over reduced catalysts. Appl Catal B Environ 2014;146:237–43. https://doi.org/10.1016/j.apcatb.2013.05.040.

[55] Gardner TH, Spivey JJ, Kugler EL, Campos A, Hissam JC, Roy AD. Structural characterization of Ni-substituted hexaaluminate catalysts using EXAFS, XANES, XPS, XRD, and TPR. J Phys Chem C 2010;114:7888–94. https://doi.org/10.1021/jp9117634.

[56] Ameen M, Azizan MT, Ramli A, Yusup S, Yasir M. Physicochemical properties of Ni-Mo/γ-Al_2O_3 catalysts synthesized via sonochemical method. Procedia Eng 2016;148:64–71. https://doi.org/10.1016/j.proeng.2016.06.496.

[57] Shtereva I, Vladov D, Rakovsky S, Ilienko B. TPS and TPR study of HDS catalysts and process mechanism. Bulg Chem Commun 2015;47:147–52.

[58] Rynkowski JM, Paryjczak T, Lenik M. On the nature of oxidic nickel phases in NiO/γ-A_l2_O3 catalysts. Appl Catal A Gener 1993;106:73–82. https://doi.org/10.1016/0926-860X(93)80156-K.

[59] Zhang J, Xu H, Jin X, Ge Q, Li W. Characterizations and activities of the nano-sized Ni/Al_2O_3 and Ni/La-Al_2O_3 catalysts for NH_3 decomposition. Appl Catal A Gener 2005;290:87–96. https://doi.org/10.1016/j.apcata.2005.05.020.

[60] Mosayebi A, Abedini R, Bakhshi H. Ni@Pd nanoparticle with core–shell structure supported over γ-Al2O3 for partial oxidation process of butane to syngas. Int J Hydrogen Energy 2017;42:18941–50. https://doi.org/10.1016/j.ijhydene.2017.06.027.

[61] Huang YJ, Xue J, Schwarz JA. Analysis of temperature-programmed reduction profiles from metal-supported catalysts. J Catal 1988;111:59–66. https://doi.org/10.1016/0021-9517(88)90065-6.

[62] Gao J, Jia C, Li J, Zhang M, Gu F, Xu G, et al. Ni/Al_2O_3 catalysts for CO methanation: Effect of Al_2O_3 supports calcined at different temperatures. J Energy Chem 2013;22:919–27. https://doi.org/10.1016/S2095-4956(14)60273-4.

[63] Torrez-Herrera JJ, Korili SA, Gil A. Structure and activity of nickel supported on hibonite-type La-hexaaluminates synthesized from aluminum saline slags for the dry reforming of methane. Chem Eng J Adv 2021;5:100080. https://doi.org/10.1016/j.ceja.2020.100080.

[64] Jeništová K, Hachemi I, Mäki-Arvela P, Kumar N, Peurla M, Čapek L, et al. Hydrodeoxygenation of stearic acid and tall oil fatty acids over Ni-alumina catalysts: Influence of reaction parameters and kinetic modelling. Chem Eng J 2017;316:401–9. https://doi.org/10.1016/j.cej.2017.01.117.

[65] Kumar P, Yenumala SR, Maity SK, Shee D. Kinetics of hydrodeoxygenation of stearic acid using supported nickel catalysts: Effects of supports. Appl Catal A Gener 2014;471:28–38. https://doi.org/10.1016/j.apcata.2013.11.021.

[66] Chen H, Wang Q, Zhang X, Wang L. Effect of support on the NiMo phase and its catalytic hydrodeoxygenation of triglycerides. Fuel 2015;159:430–5. https://doi.org/10.1016/j.fuel.2015.07.010.

[67] Fan X, Liu D, Zhao Z, Li J, Liu J. Influence of Ni/Mo ratio on the structure-performance of ordered mesoporous Ni-Mo-O catalysts for oxidative dehydrogenation of propane. Catal Today 2020;339:67–78. https://doi.org/10.1016/j.cattod.2019.02.036.

[68] Muangsuwan C, Kriprasertkul W, Ratchahat S, Liu CG, Posoknistakul P, Laosiripojana N, et al. Upgrading of Light Bio-oil from Solvothermolysis Liquefaction of an Oil Palm Empty Fruit Bunch in Glycerol by Catalytic Hydrodeoxygenation Using NiMo/Al_2O_3 or CoMo/Al_2O_3 Catalysts. ACS Omega 2021;6:2999–3016. https://doi.org/10.1021/acsomega.0c05387.

[69] Richardson JT, Scates RM, Twigg MV. X-ray diffraction study of the hydrogen reduction of NiO/ α-A_l2_03 steam reforming catalysts. Appl Catal A Gener 2004;267:35–46. https://doi.org/10.1016/j.

[70] Lock ISM, Lock SSM, Vo DVN, Abdullah B. Influence of palladium on Ni-based catalyst for hydrogen production via thermo-catalytic methane decomposition. Chem Eng Trans 2017;57:343–8. https://doi.org/10.3303/CET1757058.

[71] Luo MF, Hou ZY, Yuan XX, Zheng XM. Characterization study of CeO_2 supported Pd catalyst for low-temperature carbon monoxide oxidation. Catal Letters 1998;50:205–9. https://doi.org/10.1023/a:1019023220271.

[72] Bykova MV, Ermakov DY, Kaichev VV, Bulavchenko OA, Saraev AA, Lebedev MY, et al. Ni-based sol-gel catalysts as promising systems for crude bio-oil upgrading: Guaiacol hydrodeoxygenation study. Appl Catal B Environ 2012;113:296–307. https://doi.org/10.1016/j.apcatb.2011.11.051.

[73] Babu NS, Lingaiah N, Gopinath R, Reddy PSS, Prasad PSS. Characterization and reactivity of alumina-supported Pd catalysts for the room-temperature hydrodechlorination of chlorobenzene. J Phys Chem 2007;C:6447–53. https://doi.org/10.1021/jp065866r.

[74] Mendez CM, Olivero H, Damiani DE, Volpe MA. On the role of Pd β-hydride in the reduction of nitrate over Pd based catalyst. Appl Catal B Environ 2008;84:156–61. https://doi.org/10.1016/j.apcatb.2008.03.019.

[75] Yongwoo K, Jonghyun K, Do Heui K. Investigation on the enhanced catalytic activity of a Ni-promoted Pd/C catalyst for formic acid dehydrogenation: Effects of preparation methods and Ni/Pd ratios. RSC Adv 2018;8:2441–8. https://doi.org/10.1039/c7ra13150j.

[76] Borowiecki T, Gac W, Denis A. Effects of small MoO_3 additions on the properties of nickel catalysts for the steam reforming of hydrocarbons: III. Reduction of Ni-Mo/Al_2O_3 catalysts. Appl Catal A Gener 2004;270:27–36. https://doi.org/10.1016/j.apcata.2004.03.044.

[77] Basha SJS, Vijayan P, Suresh C, Santhanaraj D, Shanthi K. Effect of order of impregnation of Mo and Ni on the hydrodenitrogenation activity of NiO-MoO_3/AlMCM-41 catalyst. Ind Eng Chem Res 2009;48:2774–80. https://doi.org/10.1021/ie800932u.

[78] Osakoo N, Henkel R, Loiha S, Roessner F, Wittayakun J. Comparison of PdCo/SBA-15 prepared by co-impregnation and sequential impregnation for Fischer-Tropsch synthesis. Catal Commun 2015;66:73–8. https://doi.org/10.1016/j.catcom.2015.03.020.

[79] Crisafulli C, Scirè S, Maggiore R, Minicò S, Galvagno S. Co_2 reforming of methane over Ni–Ru and Ni–Pd bimetallic catalysts. Catal Letters 1999;59:21–6. https://doi.org/10.1023/A:1019031412713.

[80] Nava R, Morales J, Alonso G, Ornelas C, Pawelec B, Fierro JLG. Influence of the preparation method on the activity of phosphate-containing CoMo/HMS catalysts in deep hydrodesulphurization. Appl Catal A Gener 2007;321:58–70. https://doi.org/10.1016/j.apcata.2007.01.038.

[81] Fang G, Shaoqing G, Zegang Q, Liangfu Z, Hongwei X. Effects of impregnation methods and drying conditions on quinoline hydrodenitrogenation over Ni-W based catalysts. J Braz Chem Soc 2014;25:750–8. https://doi.org/10.5935/0103-5053.20140035.

[82] Garcia T, Weng W, Solsona B, Carter E, Carley AF, Kiely CJ, et al. The significance of the order of impregnation on the activity of vanadia promoted palladium-alumina catalysts for propane total oxidation, Catal. Sci Technol 2011;1:1367–75. https://doi.org/10.1039/c0cy00032a.

[83] Liu Q, Wang A, Wang X, Gao P, Wang X, Zhang T. Synthesis, characterization and catalytic applications of mesoporous γ-alumina from boehmite sol. Microporous

Mesoporous Mater 2008;111:323–33. https://doi.org/10.1016/j.micromeso.2007.08.007.
[84] Dhanala V, Maity SK, Shee D. Roles of supports (γ-Al2O3, SiO2, ZrO2) and performance of metals (Ni Co, Mo) in steam reforming of isobutanol. RSC Adv 2015;5:52522–32. https://doi.org/10.1039/c5ra03558a.
[85] Xing W, Li F, Yan ZF, Lu GQ. Synthesis and electrochemical properties of mesoporous nickel oxide. J Power Sources 2004;134:324–30. https://doi.org/10.1016/j.jpowsour.2004.03.038.